2018 年 8 月
博士學位論文
論文

2018年 8月 博士學位論文

Synthesis and characteristics of synthetic bone graft substitutes derived from the shell of *Haliotis* sp.

전복 패각 유래 합성골 이식재의 합성 및 특성 분석

朝鮮大學校 大學院

齒醫生命工學科

康 倧 綠

강 경 록

전복 패각 유래 합성골 이식재의 합성 및 특성 분석

Synthesis and characteristics of synthetic bone graft substitutes derived from the shell of *Haliotis* sp.

2018 年 8 月 24 日

朝鮮大學校 大學院

齒醫生命工學科

康 倧 綠

Synthesis and characteristics of synthetic bone graft substitutes derived from the shell of *Haliotis* sp.

指導敎授 金 秀 官

이 論文을 理學 博士學位신청 論文으로 提出함.

2018 年 4 月

朝鮮大學校 大學院

齒醫生命工學科

康 倧 綠

康倧綠의 博士學位論文을 認准함

委員長　朝鮮大學校　敎　授　김도경　印

委　員　서울大學校　敎　授　김영균　印

委　員　朝鮮大學校　敎　授　이숙영　印

委　員　朝鮮大學校　敎　授　김재성　印

委　員　朝鮮大學校　敎　授　김수관　印

2018 年 6 月

朝鮮大學校 大學院

CONTENTS

List of Tables

List of Figures

List of Abbreviations

3-(4,5-dimethyl thiazol-2yl)-2,5-diphenyl tetrazolium bromide	MTT
4′6′-diamidino-2-phenyl indole dihydro chloride	DAPI
Autogenous bone	Autologous
Beta-tricalcium phosphate	β-TCP
Calcium	Ca
Calcium Carbonate	$CaCO_3$
Calcium Hydroxide	$Ca(OH)_2$
Carbon Dioxide	CO_2
Distilled Water	D.W
Dulbecco's Modified Eagle's Medium	DMEM
Dulbecco's Phosphate-Buffered Saline	DPBS
Energy Despersive X-Ray Spectroscopy	EDS
Fetal Bovine Serum	FBS
Fourier Transfrom Infrared Spectroscopy	FT-IR
Guided Bone Regeneration	GBR
Hematoxylin & Eosin	H&E
Hydroxyapatite	HA
Institutional Animal Care and Use Committee	IACUC
Korea Cell Line Bank	KCLB
MG-63 osteobalst like cells	MG-63
Micro-Computed Tomography	Micro-CT
Ministry of Food and Drug Safety	MFDS
Oxygen	O
Phosphate	P
Phosphoric Acid	H_3PO_4
Revolution Per Minute	RPM
Scanning Electron Microscope	SEM
Standard Deviation	SD
X-Ray Diffraction	XRD

국문초록

전복 패각 유래 합성골이식재의 합성 및 물리·화학적 특성

강경록

지도교수 : 김수관

조선대학교 치의생명공학과 박사과정

노령 인구 및 구강 질환 환자의 증가 및 임플란트 이식 시술의 발전으로 치조골 재생용 골이식재 개발의 필요성이 대두되고 있다. 치주 질환 치료 방법 중의 하나인 임플란트 이식 시술이 보편화됨에 따라서 고가의 수입 치과 의료용 골이식재는 의료비용 상승의 원인이 되고 있다. 국민 구강 보건 향상을 위한 경제적인 치과 의료용 골이식재의 개발로, 치과 치료비용 감소 방안이 절실히 요구되는 시점이다. 또한 합성골이식재 수요 증가가 예상됨에 따라, 생물학적 안정성 및 우수한 골 형성능을 확보한 경제적인 치과 의료용 합성골이식재 원천 기술 개발 중요성은 더욱 높아지고 있는 추세이다.

본 연구에 목적은 전복 패각으로부터 베타-제삼인산칼슘(β-Tricalcium phosphate, β-TCP)과 수산화인회석(Hydroxapatite, HA)을 합성하여, 이를 원료로 한, 전복 패각 유래 합성골이식재 (HA : β-TCP = 20% : 80%)에 대한 물리·화학적 특성과 생물학적 안정성 평가를 통하여 향후, 치과 의료용 합성골이식재 개발 관련 효용성 분석을 목적으로 한다. 이에 따라 전복 패각으로부터 합성된 합성골이식재 분석을 위하여 한국 식품 의약품 안전처와 한국 식품의약품 안전평가원에서 제공되는 의료기기 평가가이드라인에 의거하여 생물학적, 물리·화학적 특성 분석을 시행하였다.

수집한 전복 패각 표면의 오염물 제거를 위하여, 초음파세척기(JAC-4020, KODO, Seoul, Republic of Korea)에서 초음파 세척을 실시한 후, 이로부터 확립된 합성 공정에 따라 β-TCP와, HA를 합성하였다. 합성된 전복 패각 유래 β-TCP와 HA를 80% : 20% 비율로 하여, 합성골이식재 제작 후, 이에 대한 물리·화학적 특성 분석 및 생물학적 안전성을 분석 하였다.

합성된 전복 패각 유래 합성골이식재는 주사전자현미경(SEM, JSM 840-A, JEOL co., Japan)으로 표면 형상 및 거칠기, 다공성 구조를 분석 하였으며, 에너지 분광분석기(Energy-Dispersive Spectroscopy, EDS, XS-169, Japan)를 통하여, 제조된 합성골이식재의 Ca/P 비율을 측정하였다. 또한 구조 결절성 분석을 위하여 X-선 회절분석을 실시하였으며, 적외선 분광 분석기(Fourier transform infrared spectroscopy, FT-IR; Nicolet 6700, Thermo Electron, USA)를 사용하여 제조된 합성골이식재의 화학적 작용기를 분석하였다.

세포 배양은 Dulbecco's modified Eagle's medium (DMEM, Life Technologies, GRAND Island, NY, USA)배지에 10% (w/v) Fetal Bovine Serum (FBS, Life Technologies, Grand Island, USA)을 혼합하여 5% CO_2가 공급되는 37℃, CO_2 배양기에서 48 시간 배양하여 사용하였다. 세포독성 평가를 위하여 MTT assay, Cell Live/Dead assay를 수행 하였으며, Alizarine Red S (Sigma-Aldrich Corp., St. Louis, MO, USA) 염색을 수행하여 골모세포의 무기질화를 분석하였다.

전복 패각 유래 합성골이식재는 주사전자현미경 관찰 시 적절한 다공성 구조와, 거칠기를 나타내는 것을 확인 할 수 있었다. EDS 분석을 통한 원소 분석 결과, 모든 성분이 시판되고 있는 합성골이식재와 동일하였으며, 시료 내의 Ca/P 비율 또한 거의 동일함을 확인 할 수 있었다. XRD를 실시하여, 결정성 분석 결과, 시판되고 있는 대조군과의 결정성이 동일함을 확인 하였다. 더불어 화학적 작용기 확인을 위한 적외선 분광 분석 결과, 시판중인 대조군과 동일한 화학적 작용기를 확인 하였다.

합성된 합성골이식재의 생물학적 안전성 평가를 위하여 실시한 MTT 및 Cell Live/Dead assay 분석 결과 제조된 합성골이식재의 세포 생존율은 88.1 ± 0.99%로, 시판되는 합성골이식재의 세포 생존율 86.36 ± 0.95% 이상의 높은 세포 생존율을 확인 할 수 있었지만 통계학적 분석 결과 유의적인 차이는 나타나지 않았다. Alizarine Red S 염색을 통하여 제조된 전복 패각 유래 합성골이식재의 골모세포 무기질화를 확인 하였을 때, 시판되고 있는 합성골이식재 수준과 동일하였다. 또한 백서 두개골 결손 모델에 합성된 합성골이식재의 8주간 골이식 실험을 통한 골이식재로써의 골 유도능 및 전도능을 평가하였을 때, 대조군인 시판되고 있는 합성골이식재 수준의 효과를 확인 할 수 있었으며, 조직학적 분석 결과, 대조군과 동일한 수준의 신생골 형성을 확인하였다.

이와 같은 결과를 종합하였을 때, 전복 패각 유래 합성골이식재는 비교 대상인 시판되고 있는 합성골이식재와 물리· 화학적 특성이 동일하며, 높은 생물학적 안전성 및, 골 유도능 및 골 전도능을 가진 것으로 확인되었다. 이는 향후 치과 의료용 합성골이식재로써 효용 가치가 높을 뿐만 아니라, 경제성이 확보된 치괴의료용 골이식재로써의 활용도가 높아, 임플란트 치료비용 완화를 통한 국민 구강 보건 증진에 기여할 것으로 사료된다.

Ⅰ. Introduction

Due to economic growth and medical development, life expectancy has increased to over 85 years old. Therefore, population aged over 65 years old have entered an aging society that accounts for over 13.5% of the total population in 2017 and will be expected to enter a super-high aged society in 2026. Furthermore, according to the development of mass media including internet, broadcasting, and information associated with medicals, the necessities related to well-being is increased in the elderly population [1, 2].

However, aging is accompanied by chronic metabolic diseases such as diabetes, hypertension, cardiovascular diseases, and the degeneration of tissues including bone, joints, and brain. Moreover, chronic metabolic diseases and aging-dependent degenerative diseases affect the balance of oral homeostasis by increasing inflammation caused by aging. Such increased oral inflammation in the oral tissues induces periodontal bone loss through an increase in osteoclasts from macrophages, which is called osteoclastogenesis [3].

Today's surgeons and dentists face many situations that require bone grafting. More than 2,200,000 bone grafting procedures are being performed annually worldwide in order to repair bone defects in the areas of orthopedics, neurosurgery, and dentistry [4-6]. Indications for bone grafting involve fractures with bone loss, metaphyseal defects, comminution, nonunions delayed unions, and bone lesions, malunions, and arthrodesis [7]. In addition, spinal fusions and filling defects following the removal of bone tumors or occurrence of congenital diseases may require bone grafting [8].

Given the enormous scope of bone grafting, numerous methods have been developed to fulfill these needs. With the current biotechnology/tissue engineering advancements, it is only to be expected that the number of bone grafting solutions

will continue to grow [5].

From a biological point of view, bone as a living tissue is play to serve several important functions in the body. Bone not only offer structural protection and support to the body's organs, but it is involved in the metabolism of minerals such as calcium and is also a major part of the synthesis of blood cells. In addition, to meet various load demands, 'remodeling' ensures optimum shape and structure through continuous renewal process to cope with changes in mechanical environment, thus maintaining optimum function and balance among formats. Bone formation is a process of direct bone formation and exists only in cells. Osteoprogenitor cells that survive in the donor graft survive and proliferate during transplantation and may differentiate into osteoblasts and ultimately bone cells.

These cells represent "osteogenic potential" of the graft. The only substance with true osteogenic properties is autograft. Hypothetical synthetic osteogenic substitutes include osteoblasts genetically engineered in a convenient environment and provide a matrix and pattern for bone development (Fig. 1). However, as a living organization, bones need to constantly supply oxygen and nutrients, and the size of fractures and defects that can be restored in healthy tissue is limited. In addition, bone may be affected by pathological conditions and may degenerate as a result of age and disease. In this case, patient comfort, bone function can often be preserved only by surgical reconstruction. That is, "bone grafting" is required [9, 10].

Bone grafting and guided bone regeneration (GBR) are treatments used to replace teeth lost due to various reasons such as periodontal diseases. Different bone graft materials are used to prevent alveolar bone from gingival tissue from being lost. Bone grafting material is effective for bone regeneration and formation as it improves the combination of implant and bone tissue and fills a part of the lost alveolar bone defect. Consequently, bone grafting care has become an integral part of dentistry [11-14].

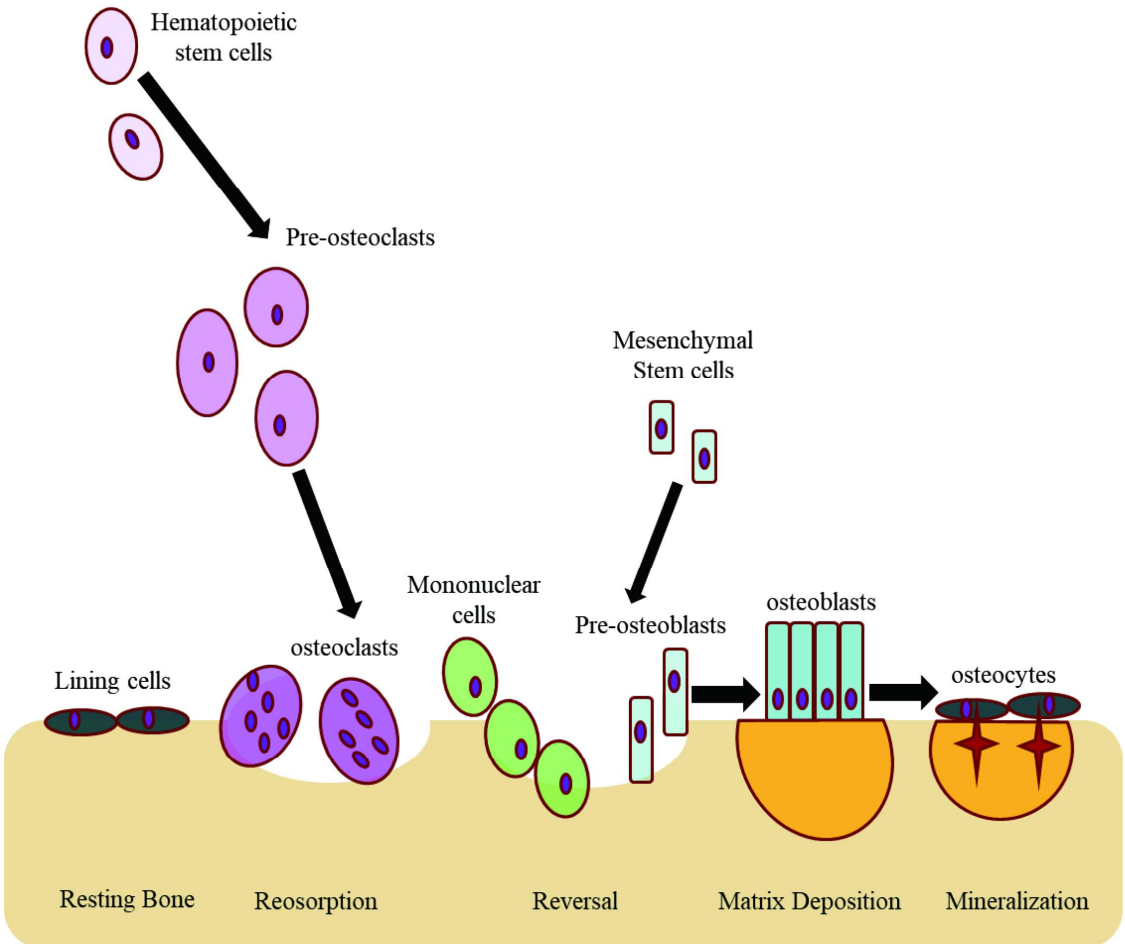

Fig. 1. Schematic diagram of the bone remodeling process.

This technique is used to promote bone regeneration when the thickness of the jawbone is insufficient for implant placement. After implant placement, the bone-defect area is filled with autogenous bone or artificial bone graft material and covered with a barrier membrane. When a large amount of bone needs to be replaced, GBR should be carried out before placing the implant. Therefore, bone grafting materials and barrier membranes are essential for bone regeneration. Among the many bone grafting materials available, synthetic bone grafting materials are the most versatile for dental clinical surgery [14,15].

Only the autologous bone grafting technique meets all these requirements. All other bone grafting materials support only a subset of these processes. Therefore, autologous bone grafting continues to be a gold standard in reconstructive surgery because it has superior osteogenic potential as compared to allogeneic transplantation [8, 16-19].

Autogenous bone (autologous) grafting involves the use of bone obtained from the individual receiving the graft. Autogenous bones are better than bone regeneration because the graft is derived from the patient's own body and is less resistant to transplant rejection. On the other hand, such surgery involves additional risks. A dental surgeon performs an incision to retrieve small bone fragments from unwanted body parts, which may be related to increased morbidity and wound site infection [6, 21-23].

Therefore, the limited availability of autologous bones is a major problem for surgeons and patients owing to which surgical treatment of large-scale bone defects is still a problem. In addition, as the number of senior patients or individuals with variable systemic medical conditions and biological drawbacks associated with the bone-healing process increases, it is associated with prosthetic implants to improve the biological fixation and bone integration process The use of bone substitutes as adjuvant therapy is required [23, 24].

Due to limitations of autografting, a demand for allogeneic bones as replacement or substitutes for autologous bones is increasing. Allografts are the most frequently selected bone substitutes and are considered the second choice of surgeons. There are numerous configurations of allograft bones available, included powder, cancellous cubes, cortical struts, cortical chips, and others [25, 26]. The increased availability of allografts makes it possible to manufacture customized molds. Allografts are prepared in lyophilized forms; fresh allogeneic transplantation is rarely used because it might generate an immune response or transmit diseases [27]. Lyophilized allografts are least immunogenic, but are inferior in osteoinductive and mechanical properties and strength when compared to frozen allografts [28]. The method of preparations are devised to minimize host's immune reaction and therefore no viable cells provide osteogenic properties in most allografts [29-33]. However, there are some problems related with the use of allogeneic transplants, such as disease transmission (viral or bacterial), tumor transplantation, and immune rejection [34].

Currently, several alternative tissues for autologous bone grafts including xenografts, xenograft-derived hydroxyapatite, synthetic calcium phosphate, bioactive glass/glass ceramic, type I collagen, degradable polymers, some matrix proteins, and various refined materials are being studied. They may include commercially available growth factors, isolated bone marrow cells, and complexes of these materials. The effectiveness of many of these materials has been demonstrated in experimental and clinical situations.

Recently, alternative tissues of autologous bone grafts such as xenografts, xenograft-derived hydroxyapatite, synthetic calcium phosphate, bioactive glass / glass ceramic, type I collagen, degradable polymers, and some matrix proteins, have been developed to use as a bone grafting materials. Furthermore, complex types of these materials combined with either bone marrow cells or anabolic growth factors were commercially developed for accelerating the bone regeneration after transplantation into defecting bone. A xenograft bone substitute is derived from a

species other than human, such as cattle or pig, and can be lyophilized or desalted and deproteinized [35].

Synthetic bone grafting materials are bone substitutes that were synthesized using calcium phosphate-based biomaterial; they are suitable for bone grafting because as calcium phosphate properties similar to those of the mineral phases of bone and teeth in the human body. Further, synthetic grafts guaranteed to be biologically safe are being studied to supplement the demerits of various bone graft materials and achieve the ideal properties required for bone regeneration.

Hydroxyapatite (HA) is a typical biomaterial known for its excellent biocompatibility, bioactivity, and osteoconductive properties in vivo, and it has a low solubility. On the other hand, beta-tricalcium phosphate (β-TCP) is a material of excellent biodegradability as it is highly soluble. But before the bone grafting material can be replaced in the tissues of the bone defect, β-TCP is quickly absorbed. Synthesized bone grafting materials and substitutes can be manufactured from ceramics, such as calcium phosphates, HA, TCP, bioglass, and calcium sulfate, all of them are biological active to different extents depends on their solubility in physiological environment [36]. These materials can be doped with growth factors, ions such as strontium, or mixed with bone marrow aspirate to increase their biological activity.

Currently, a biocompatible β-TCP powder is being synthesized from natural materials, such as eggshells, cuttlefish bones, and oyster shells. However, the shell of the abalone, a species of gastropods mainly found in East Asia [37], has the highest $CaCO_3$ (calcite) and lowest $CaCO_3$ (aragonite) content [38]. These are inorganic minerals used in the synthesis of bioceramics such as β-TCP [39].

Abalone (*Haliotis* sp.) shells are used as decorative items and as a source for jewelry, buttons, buckles, and inlays, but the vast majority of them are discarded in landfills and hence are environmental pollutants.

Table 1. Bone replacement grafts [20].

Human bone
Autogenous grafts (autografts)
Extraoral
Intraoral
Allogeneic grafts (allografts)
Fresh-frozen bone allografts
Freeze-dried bone allografts
Demineralized bone matrix allografts
Bone substitutes
Xenogeneic grafts (xenografts)
Bovine-derived hydroxyapatite
Coralline calcium carbonate
Alloplastic grafts (alloplasts)
Polymers
Bioceramics
bioactive glass, glass ceramics
β-tricalcium phosphate
Hydroxyapatite
Dense, nonporous, nonresorbable
Porous, nonresorbable
Resorbable hydroxyapatite
Biphasic calcium phosphate
Calcium phosphate bone cement

Every year, the tipping fees for the proper disposal of waste abalone shells are particularly expensive. Therefore, the recycling of waste materials using low-cost technology to produce biocompatible materials, such as bone grafting materials and their source materials, such as HA and β-TCP from abalone shells, is a significant development.

The first aim of this study is to synthesize bioceramics such as β-TCP and HA from the shells of *Haliotis* sp. and to verify the physicochemical characteristics and cellular biocompatibility of these bioceramics for use as bone grafting materials. The secondary aim of this study is to synthesize the bone grafting materials and to examine the physicochemical and biological properties of *Haliotis* sp. shell-derived bone grafting materials in dental implants.

Ⅱ. Materials and Methods

Ⅱ-A. Synthesis and characteristics of bone graft substitute

The processing steps to synthesize the bone graft Substitute from the shells of *Haliotis* sp., an abalone shells were briefly described in Fig. 2-4.

Ⅱ-A-1. Synthesis of CaO from the shell of *Haliotis* sp.

Contaminants were removed from abalone shells by washing in distilled water using ultrasonicator (KODO, JAC-4020, Republic of Korea). The *Haliotis* sp. shells were then dried for 48 h at room temperature. Completely dried the *Haliotis* sp. shells were pulverized to a powder in a blender (WB-1, Kastech, Japan). To determine the optimal sintering temperature for CaO synthesis from the *Haliotis* sp. shells, 100 g abalone shell powder was sintered in an electric furnace (MF-22G, JEIO TECH, Seoul, Republic of Korea) at 900, 950, and 1000℃ for 3 h. After sintering at various temperatures, the generated products were collected and compared with commercial CaO (Junsei Chemical Co., Ltd., Tokyo, Japan), by Fourier transform infrared spectroscopy (FT-IR; Nicolet 6700, Thermo Electron, USA) and X-ray diffractometer (XRD, X'Pert PRO MRD, PANalytical Co., Netherlands).

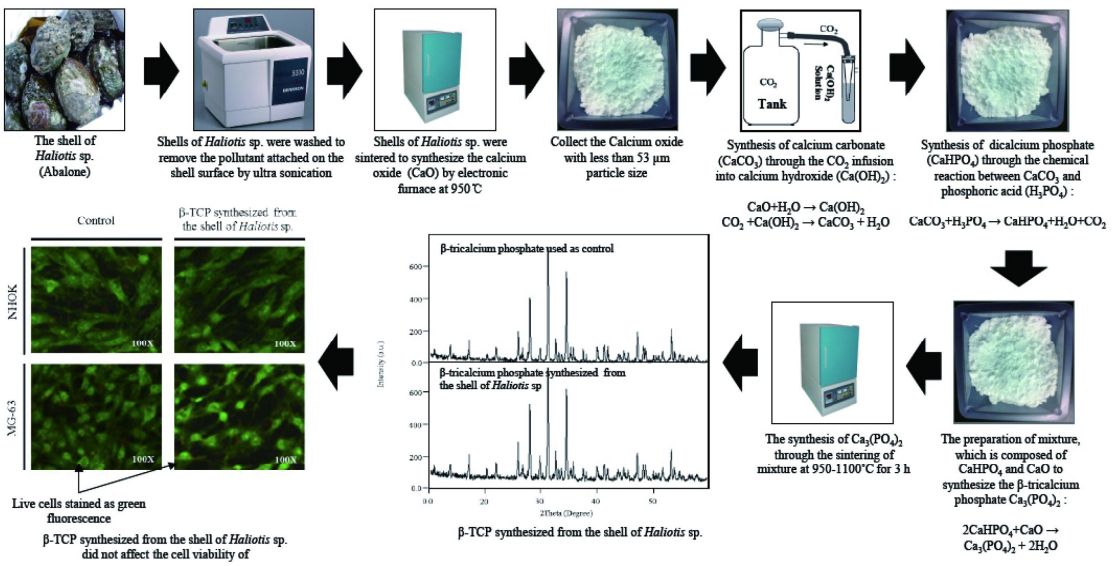

Fig. 2. A schematic diagram of the synthesis of β-TCP from the shells of *Haliotis* sp.

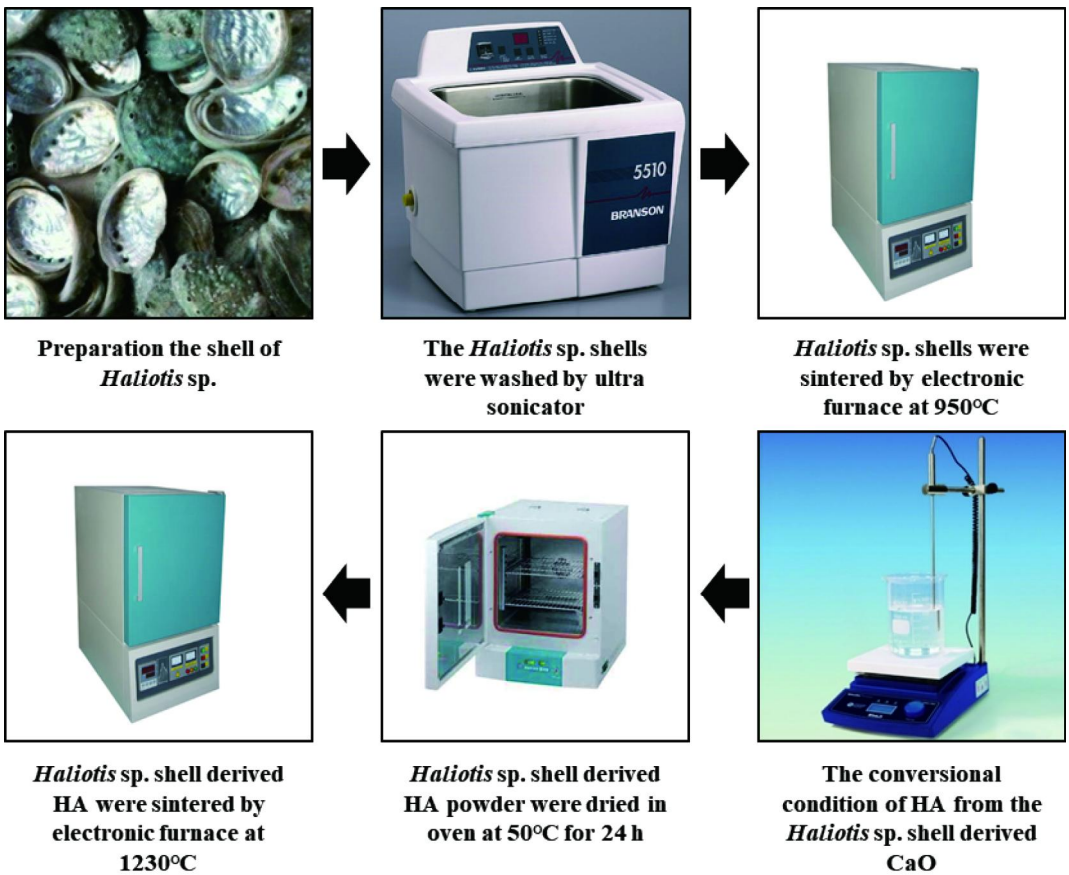

Fig. 3. The schematic diagram to synthesize the HA from the shell of *Haliotis* sp.

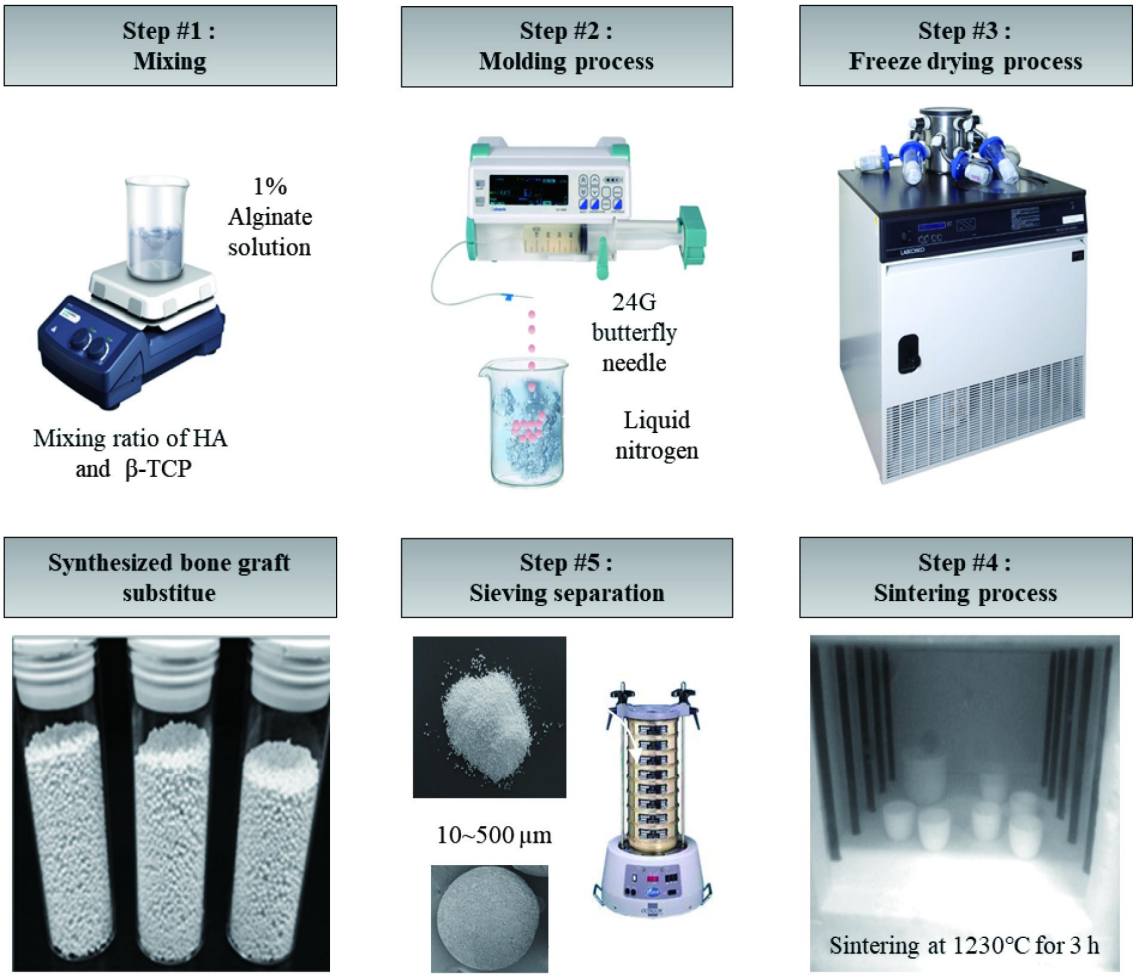

Fig. 4. Schematic diagram of the synthesis of bone grafts from the shells of *Haliotis* sp.

Ⅱ-A-2. Synthesis of $CaCO_3$ from CaO Synthesized from the shell of *Haliotis* sp.

CaO synthesized from abalone shells was pulverized to < 53-μm particles. Next, $CaCO_3$ was synthesized by a $CaCO_3$ precipitation through CO_2 infusion, based on a synthesis approach previously describedby Feng et al [40].:

$$CaO + H_2O \rightarrow Ca(OH)_2 + CO_2 \rightarrow CaCO_3$$

Briefly, to prepare the solution of calcium hydroxide [$Ca(OH)_2$], 5 g of CaO was completely dispersed in 200 mL deionized water by stirring with a magnetic bar at 250 rpm. In the second step, to synthesize and precipitate $CaCO_3$, carbon dioxide (CO_2) gas (with gas flow rate regulated at 3.5 L/min) was used to infuse the $Ca(OH)_2$ solution until pH 7.4 was reached, with controlled reaction temperature (40 ℃) and with stirring (250 rpm). The precipitated product was rinsed three times with distilled water to remove any impurities, filtered through filter paper, and dried in a drying oven at 50℃ for 24 h. Finally, the synthesized products were collected and compared with commercial $CaCO_3$ (Junsei Chemical Co., Ltd., Tokyo, Japan) by FT-IR and XRD.

Ⅱ-A-3. Synthesis of $CaHPO_4$ from $CaCO_3$ derived from the shell of *Haliotis* sp.

$CaHPO_4$ was synthesized by a chemical reaction between phosphoricacid (H_3PO_4) (Sigma-aldrich, St. Louis, MO, USA) and $CaCO_3$ using a modified procedure reported by Tas [41]. :

$$CaCO_3 + H_3PO_4 \rightarrow H_2O + CO_2 + CaHPO_4$$

Briefly, to determine the optimal pH conditions for the synthesis of $CaHPO_4$ from H_3PO_4 and $CaCO_3$, 5g $CaCO_3$ were completely dispersed in 200 mL deionized water by stirring with a magnetic bar at 250 rpm. The solution of $CaCO_3$ was sequentially adjusted to pH 6.0, 7.0, and 8.0 through slow dropwise addition of 10 % H_3PO_4 (85% solution) at room temperature, and was continuously stirred for 5 h to ensure complete reaction between $CaCO_3$ and H_3PO_4. The synthesized products were rinsed three times with distilled water to remove any impurities, filtered through filter paper, and dried completely for 24 h. Finally, synthesized products were collected and compared with commercial $CaHPO_4$ (Junsei Chemical Co., Ltd., Tokyo, Japan) by FT-IR and XRD.

Ⅱ-A-4. Synthesis of β-TCP from $CaHPO_4$ derived from the shell of *Haliotis* sp.

$Ca_3(PO_4)_2$ was synthesized by a chemical reaction between CaO and $CaHPO_4$ using a modified sintering process described previously by Chang et al [42].:

$$CaO + 2CaHPO_4 \rightarrow Ca_3(PO_4)_2 + H_2O$$

Briefly, 5 g of $CaHPO_4$ were completely dissolved in 200 mL deionized water by stirring with a magnetic bar at 250 rpm. CaO and $CaHPO_4$ were mixed at a ratio of 1 : 2 for 12 h, at room temperature. Following the reaction, the CaO and $CaHPO_4$ mixture was allowed to precipitate for 12 h at room temperature. To separate the sediment from the CaO and $CaHPO_4$ mixture, the supernatant was discarded. The collected sediment was dried at 50℃ for 24 h. However, to verify the optimal sintering temperature for the synthesis of $Ca_3(PO_4)_2$, the collected sediment was sintered in an electric furnace (MF-22G, Jeio Tech Co., Ltd, Seoul, Republic of Korea) at 950, 1000, 1050, or 1100℃ for 3 h. Finally, the synthesized products were collected and compared with commercial β-TCP (Sigma-aldrich, St. Louis, MO, USA) by FT-IR and XRD.

Ⅱ-A-5. Synthesis of HA from the shell of *Haliotis* sp.

The *Haliotis* sp. shells used in this study were collected randomly from a commercial seafood market in Wando, Republic of Korea. The contaminants attached to the abalone shells were removed by using an ultrasonicator (JAC-4020, KODO, Seoul, Republic of Korea) for 1 h at room temperature; this step was repeated three times. Sequentially, the *Haliotis* sp. shell were washed with hydrogen peroxide in an ultrasonicator for 90 min at room temperature. To rinse the hydrogen peroxide, the *Haliotis* sp. shells were washed with the ultrasonicator for 1 h at room temperature. The *Haliotis* sp. shells were then dried for 48 h at room temperature and then crushed to powders in a wonder blender (KT. WB-1, Kastech, Japan). To synthesize CaO, the *Haliotis* sp. shell powder was sintered in an electronic furnace (MF-22G, JEIO TECH, Seoul, Republic of Korea) at 950°C for 3 h. After sintering, CaO, ≤ 53 μm in size, was collected using a mesh-sieve. Finally, the synthesized residues were investigated by a comparison with commercial CaO (Sigma-Aldrich Corp., St. Louis, MO, USA). To synthesize calcium hydroxide [$Ca(OH)_2$], the CaO sintered from the *Haliotis* sp. shells were dissolved in distilled water by stirring with a magnetic bar at 300 rpm. After dissolution, 0.3 M phosphoric acid wa s added drop-wise into the $Ca(OH)_2$ solution at pH 10.5. The reacted residues were washed with DW to remove the impurities, filtered through filter paper, and dried in a dry oven at 50℃ for 24 h. Finally, the residues were sintered in an electronic furnace at 1230℃ for 3 h. After the sintering process, there sidues were investigated by a comparison with commercial HA (Sigma-Aldrich Corp., St. Louis, MO, USA)

Ⅱ-A-6. Synthesis of Bone graft substitute from the shell of *Haliotis* sp.

In our study, we used the *Haliotis* sp. shell-derived HA and *Haliotis* sp. shell-derived β-TCP powders at a ratio of 2 : 8. We used alginate solution as the binder. The powders were mixed in a beaker at the appropriate ratio with a 1% alginate solution and stirred. The resulting slurry had a certain degree of viscosity and was drop wised into liquid nitrogen by syringe pump with 21 G butterfly needle. Harvested beads of bone graft materials was lyoplized for 48 h at freezing dryer and then sintered to 1230℃ by increasing the temperature at 100℃/h. and followed subsequent slow cooling to room

Ⅱ-B. Evaluation of physical and chemical properties

Ⅱ-B-1. Scanning electron microscopy analysis

To observe the morphology of the synthesized materials, prepared samples were coated by sputter-coated (Emitech K550 sputter coater, Emitech Ltd, UK) and were observed by scanning electron microscope (SEM, JSM 840-A, JEOL co., Japan) at 1000X, 3000X, and 1000X magnifications. The Ca/P ratio was examined by energy dispersive spectrometry (EDS, XS-169, Japan).

Ⅱ-B-2. X-ray diffraction and fourier transform infrared spectroscopy analysis

The crystal structure of the materials was determined by X-ray diffraction (XRD, X'pert PRO MRD, PAN alytical co. The Netherlands) using CuK_a radation produced at 40 kV and 30 mA. The patterns were scanned from 10° - 60° 2θ at a scan rate of 2° per minute with a step size of 0.05°. The chemical characteristics were measured by Fourier-transform infrared (FT-IR; Nicolet 6700, Thermo Electron, USA) sperctroscopy.

Ⅱ-B-3. pH of synthetic bone graft substitute

The pH of bone grafting substitutes synthesized as defined mixing ratio of HA and β-TCP by both the pH paper and the pH meter. The pH values of effluents of each bone graft substitutes prepared by regarding guidelines supplied by ministry of food and drug safety (MFDS), Republic of Korea, were analyzed by pH meter. The pH values of Eluted solution of each bone graft materials were visualized by pH test paper.

Ⅱ-B-4. Dissolution Ratio test

The solubility of each synthesized bone graft materials synthesized as the defined mixing ratio of *Haliotis* sp. shell-derived HA and *Haliotis* sp. shell-derived β-TCP. The solubility of bone graft material was measured by the protocol provided by MFDS, Republic of Korea.

Ⅱ-B-5. wettability test

The wettability of each bone grafting substitutes synthesized as the defined mix ratio of HA and β-TCP. The wettability of bone grafting material was measured by the protocol provided by MFDS, Republic of Korea. Briefly, synthesized bone grafting substitutes were immersed with the distilled water at room temperature for 30 min. After reaction, the remained distilled water was analyzed by the microbalance.

Ⅱ-C. *In vitro* cytocompatibility

Ⅱ-C-1. Cell culture

Human MG-63 osteosarcoma cells (MG-63 cells) were obtained from Korea cell line bank (KCLB, Seoul, Republic of Korea). MG-63 cells were cultured in the Dulbecco's modified Eagle's medium (DMEM, Life Technologies, GRAND Island, NY, USA) supplemented with 10% fetal bovine serum (FBS, Life Technologies, Grand Island, NY, USA) in humidified atmosphere containing 5% CO_2 at 37℃.

Ⅱ-C-2. Analysis of cell cytotoxcity

To verify the biological safety of synthesized materials from *Haliotis* sp., 0.2 mg synthesized materials was eluted into culture media containing 10% FBS for 72 h at 37℃. In addition, the same amount of commercial β-TCP and HA and Bone graft substitutes were used as control and was eluted by the same procedure. The cytotoxicity of synthesized materials were assessed using 3-(4,5-dimethyl thiazol-2-yl)-2, 5-diphenyl tetrazolium bromide (MTT) assay. Briefly, cells were cultured to density of 1 X 10^5 cells/mL in the 96-well culture plates and were allowed for 24 h in a humidified incubator at 37 ℃ in 5% CO_2. The cultured cells were treated for 24 h with 200 μL of each eluent prepared from the control and synthesized materials. There after, 20 μL 5 mg/mL MTT was added. After 4 h, the supernatant was removed, and MTT crystals were dissolved in dimethylsulfoxide (200 μL/well). Finally, optical density was measured at 570 nm using a spectrometer (Epoch Micro-volume Spectro photometer System, BioTek, VT, USA). The experiments were performed at least three times.

Ⅱ-C-3. Analysis of cell viability

We determined whether the Ca^{2+} eluted from synthesized materials from *Haliotis* sp. shell induced apoptotic cell death. Morphological alteration of cell nuclei was assessed using a modified 4'6'-diamidino-2-phenyl indole dihydro chloride (DAPI) staining in MG-63 cells stimulated with eluent of synthesized materials from *Haliotis* sp. shell. Briefly, MG-63 cells were stimulated with each eluent for 24 hr in the humidified incubator at the 37℃ in 5% CO_2. Thereafter, the cell was washed with Dulbecco's phosphate-buffered saline (DPBS) after removing the medium. The cell was fixed by in the 4% paraformaldehyde for 20 min and was observed by fluorescence microscopy (Eclipse TE2000, Nikon Instruments, NY, USA). Furthermore, live and dead cell assay was performed using green calcein AM and ethidium homodier-1 (Life Technologies, Grand Island, NY, USA) to stain live and dead cells, respectively. To evaluate cell survival, cells were plated on chamber slides and were treated for 24 h with eluents prepared from synthesized materials. Thereafter, cell survival assays were performed according to the manufacturer's protocol.

Ⅱ-C-4. Alizarine Red staining

The MG-63 cell was fixed with 70% ethanol for 15 min and stained with 1% of the Alizarin red S solution (Sigma-Aldrich Corp., St. Louis, MO, USA) in 0.1% NH_4OH at pH 4.2 - 4.4. The mineralization assays were performed by staining MG-63 cells with Alizarin red S solution.

Ⅱ-D. *In vivo* osteoinductivity

The experimental procedure to determine the biological safety and osteoconduction of Bone graft substitutes in animal model with calvarial bone defection were briefly described in Fig. 5.

Ⅱ-D-1. Housing conditions of experimental animals

Experiment animal selection and management, surgical procedure, and preparation were performed by protocol (CDMDIRB 1008A60) approved by Institutional Animal Care and Use Committee (IACUC) of Chosun University, Gwangju Republic of Korea. In present study, Sprague-Dawley rats (weight 200 to 300 g) were maintained in a clean room controled with 12 h day/night cycles, the temperature of 20℃, and *ad libitum* approach water and the standard laboratory pellet diet.

Ⅱ-D-2. Surgical generation of experimental animals with calvarial bone defection

Animals were anaesthetized by the intramuscular injection using Zoletile (15 mg/kg; Virbac, Virbac Korea, Republic of Korea). Routine infiltration anaesthesia using 2.0% Lidocaine (epinephrine 1:100000, lidocaine HCl, Huons, Republic of Korea) were performed at the surgical area. Sequentially, surgical areas were shaved to remove hair and were sterilized using betadine to prevent contamination.

A standardized and transosseous defect, circular 8 mm in the diameters, were performed on the calvarial bone with the used of the DPBS cooled trephine bur. After removal of the trephined calvarial disk, sterilized bone grafting substitute was covered on the defecting sites of cranium evenly without suture.

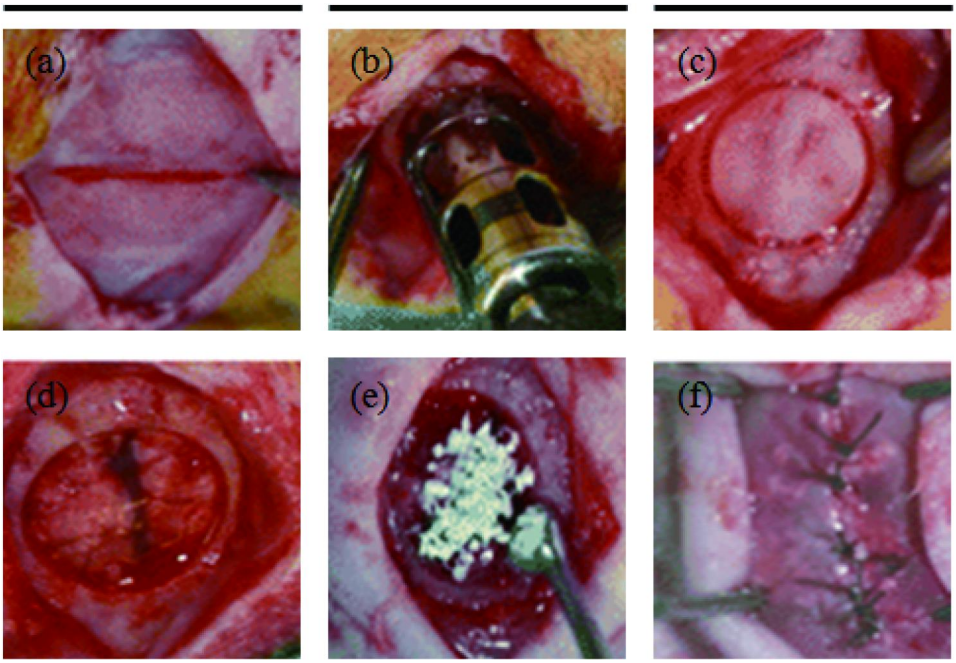

Fig. 5. Experimental calvarial bone defect animal modeling procedure. The experimental procedure to detemine the biological safety and osteconduction of synthetic bone graft substitutes in animal model with calvarial bone defection. Animal selection and management, surgical procedures, and preparation were performed according to experimental protocol approved by Institutional Animal Care and Use Committee (IACUC) of Chosun University, Gwangju, Republic of Korea.

The periosteum and skin was then closed and suturing with 4-0 coated polygalactin. Experimental animals were sacrificed at 8 weeks post-surgery by CO_2 asphyxiation. Calvarial bones dissected from each animals were fixed by 4% paraformaldehyde for 7 days at 4℃ to perform histological and the radiographic evaluation.

Ⅱ-D-3. Radiographic evaluation

Ⅱ-D-3-a. Analysis of X-ray image

Dissected from the each animals calvarial bone were analyzed using the MX-20 Specimen Radiography System (Faxitron Bioptics LLC, Lincolnshire, IL, USA). The regeneration of bone defecting area applied with bone graft substitutes were radiographied by placing the calvarial bones dissected directly on X-ray for 5 min with the energy for 10 kV. The images were digitized, and the defecing area regeneration were evaluated.

Ⅱ-D-3-b. Analysis of micro-CT image

At the defecting area on the calvarial bone was anlyzed by the microscope examination and the Micro-Computed Tomography (micro-CT) scanning. Dissected calvarial bone was immediately fixed by the 4% paraformaldehyde, followed by Micro-CT image analysis conducted using the SkyScan 1076 (SkyScan, Konitch, Belguim) with energy for 130 kV and rotation step 0.2°.

Ⅱ-D-4. Histological evaluation

calvarial bone of experimental animals were excised and post-fixed by the 4% paraformaldehyde for 10 days, dehydrated in series of ethanol solutions (50 - 100%) at 20 min per step, and then soaked in xylene. For conventional the histological stain, paraffin-embedded tissue block was prepared and sectioned at 10 ㎛ thickness with the microtome (Leica Microsystems AG, Wetzler, Germany) on superfrost plus slides (Menzel, Braunschweig, Germany). After deparaffinization in the xylene for 35 min, section was hydrated through the gradients with the decreasing proportions of ethanol. The bone paraffin sections were stained with hematoxylin and eosin (H&E) stain and safranin-O and fast green stain at the 4X modifications to show the calvarial defecting areas.

Ⅱ-D-4-a. Hematoxylin & Eosin staining

Bone defecting areas were analyzed after H&E stain (Sigma-Aldrich, Gillingham, UK). The bone paraffin sections were stained by H&E stain at the 4X modifications to show the calvarial defect areas by microscopy.

Ⅱ-D-4-b. Safranin-O & fast green staining

The proteoglycan contents of the bone was analyzed following safranin-O & Fast green stain (Sigma-Aldrich, Gillingham, UK). The bone paraffin sections stained with safranin-O & fast green staining at 4X modifications to observe the calvarial defect areas by microscopy.

Ⅱ-E. Statistical analysis

The experimental datas were presented as mean ± standard deviation (SD) from

at the least of three independent experiments and were analyzed using the analysis of variance, followed by the Student's t-test. The p-value of less than 0.05 were considered statistically significant.

Ⅲ. Results

Ⅲ-A. Synthesis and characteristics of bone graft substitutes

Ⅲ-A-1. FT-IR and XRD characterization of CaO synthesized from the *Haliotis* sp. shell

To determine the optimal sintering temperature for CaO synthesis from abalone shells, sintering was conducted in an electric furnace at temperatures of 900, 950, and 1000℃ for 3 h. The composites synthesized at each sintering temperature were analyzed by FT-IR and XRD. As shown in Fig. 6, the FT-IR results revealed a sharp band at 3656 cm^{-1}, two broad weak bands centered at approximately 3822 and 3388 cm^{-1}, a medium doublet centered at around 1444 cm^{-1}, and a very strong absorption below 600 cm^{-1} for all the synthesized composites. The band profile of the composite obtained by sintering at 950℃ was matched with that of commercial CaO, which is used as a control. Furthermore, to verify the conversion from abalone shells to CaO, the composite synthesized by sintering at 950℃ was analyzed by XRD, as shown in Fig. 7. The XRD patterns of commercial (control) CaO were observed at 32.24°, 37.4°, and 53.92°. The XRD spectra of CaO derived from abalone shells by sintering at 950℃ matched the peaks of commercial CaO. These results indicated that CaO was successfully synthesized from abalone shells by sintering at 950℃ for 3 h.

Ⅲ-A-2. FT-IR and XRD characterization of $CaCO_3$ from CaO synthesized from *Haliotis* sp. shell

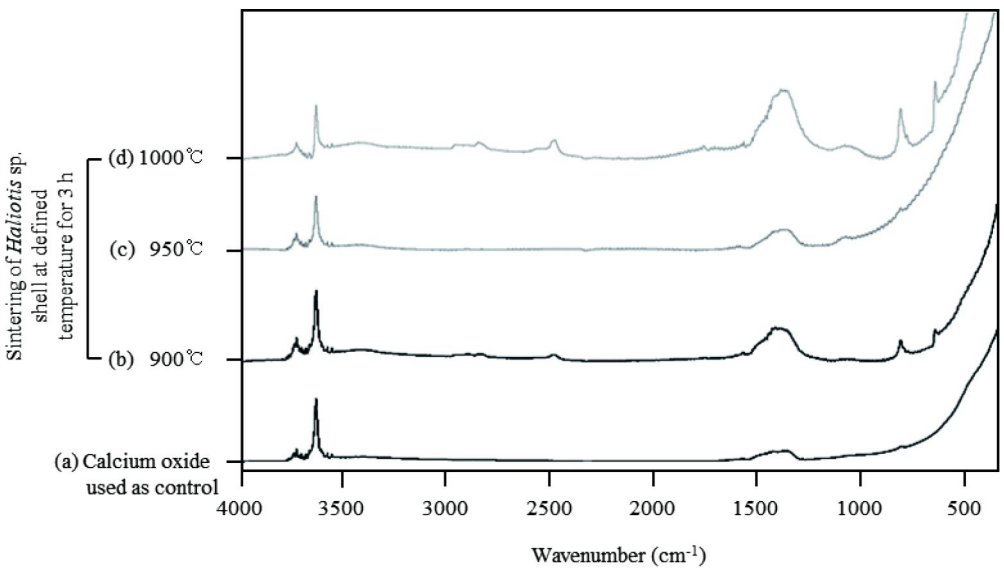

Fig. 6. FT-IR analysis of CaO synthesized from the shell of *Haliotis* sp. (a) spectrum of control CaO commercially purchased and spectra of CaO sintered at (b) 900, (c) 950, and (d) 1000℃.

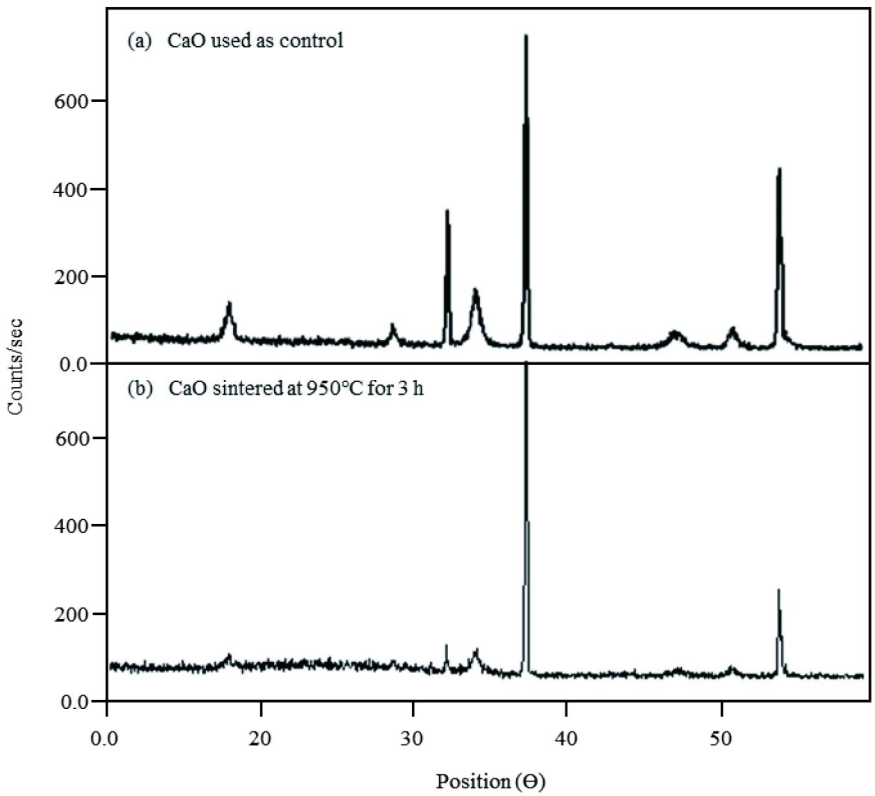

Fig. 7. XRD analysis of *Haliotis* sp. shell-derived CaO sintered at 950℃. The crystal structure of the materials was determined by XRD using CuK_a radiation at 40 kV and 30 mA. The samples were scanned from 10° - 60° 2Θ at a scan rate of 2°/min with a step size of 0.05°. (a) Peaks of control CaO commercially purchased and (b) peaks of CaO sintered at 950℃

To synthesis $CaCO_3$ from CaO derived from *Haliotis* sp. shells, CO_2 gas was injected into $Ca(OH)_2$ solution, which was prepared by resuspension of CaO into distilled water. The composites synthesized by CO_2 gas injection into $Ca(OH)_2$ solutions were analyzed by FT-IR and XRD to verify the conversion of $CaCO_3$ from CaO. As shown in Fig. 8, the FT-IR spectrum of commercial $CaCO_3$ used as the control exhibited bands at 713, 875, and 1418 cm^{-1} corresponding to the asymmetrical stretching vibration peaks of O-C-O. These are well-known characteristic peaks of calcite [43, 44]. Moreover, $CaCO_3$ synthesized by the infusion of CO_2 gas into $Ca(OH)_2$ derived from *Haliotis* sp. shells exhibited the same bands as commercial $CaCO_3$. Furthermore, the XRD spectrum of commercial $CaCO_3$ used as the control showed characteristic diffraction peaks at 23.09°, 29.40°, 36.0°, 39.43°, 43.18°, and 48.52°, as shown in Fig. 9. All of these peaks indicate the formation of a calcite phase [45]. Moreover, the XRD spectrum of $CaCO_3$ derived from the *Haliotis* sp. shells matched that of commercial $CaCO_3$. Therefore, these results indicate that $CaCO_3$ was synthesized successfully from *Haliotis* sp. shells by the infusion of CO_2 into a $Ca(OH)_2$ solution. Approximately 4.5 g of $CaCO_3$ was collected from 5 g of CaO derived from *Haliotis* sp. shells by CO_2 infusion.

Ⅲ-A-3. FT-IR and XRD characterization of $CaHPO_4$ from $CaCO_3$ synthesized from *Haliotis* sp. shell

$CaHPO_4$ was synthesized by the chemical reaction of H_3PO_4 and *Haliotis* sp. shell-derived $CaCO_3$. To determine the optimal pH conditions, chemical reactions between H_3PO_4 and $CaCO_3$ were performed at pH 6.0, 7.0, and 8.0. Thereafter, the chemical properties of the synthesized composites were examined by FT-IR and XRD. As shown in Fig. 10(a), the broad absorption peak between 2400 to 3500 cm^{-1} results from O-H stretching vibrations. H-O-H bending leads to an absorption peak at

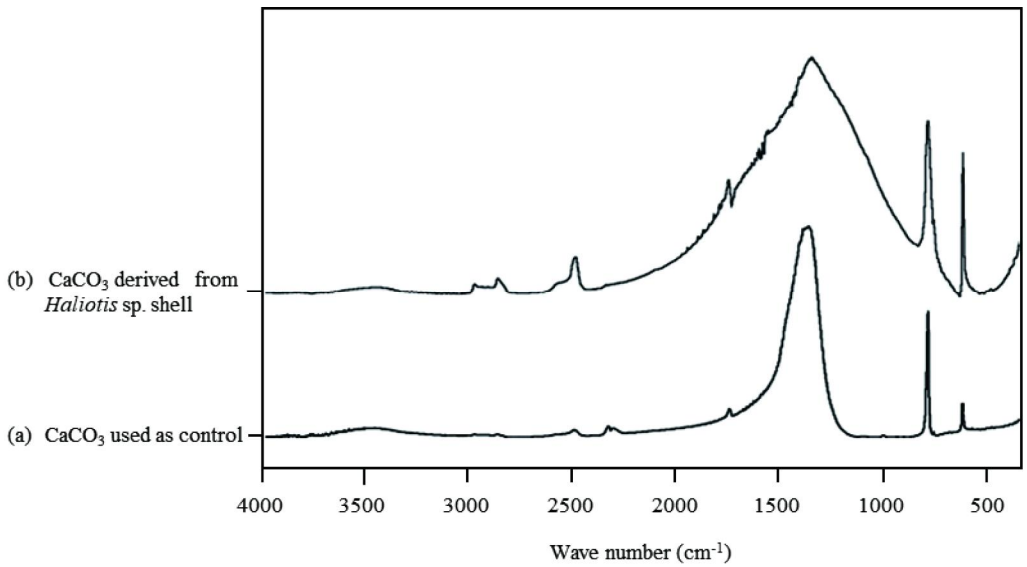

Fig. 8. FT-IR analysis of $CaCO_3$ synthesized from *Haliotis* sp. shell-derived CaO by the infusion of CO_2. Spectra of (a) control $CaCO_3$ commercially purchased and (b) $CaCO_3$ derived from *Haliotis* sp. shell derived CaO.

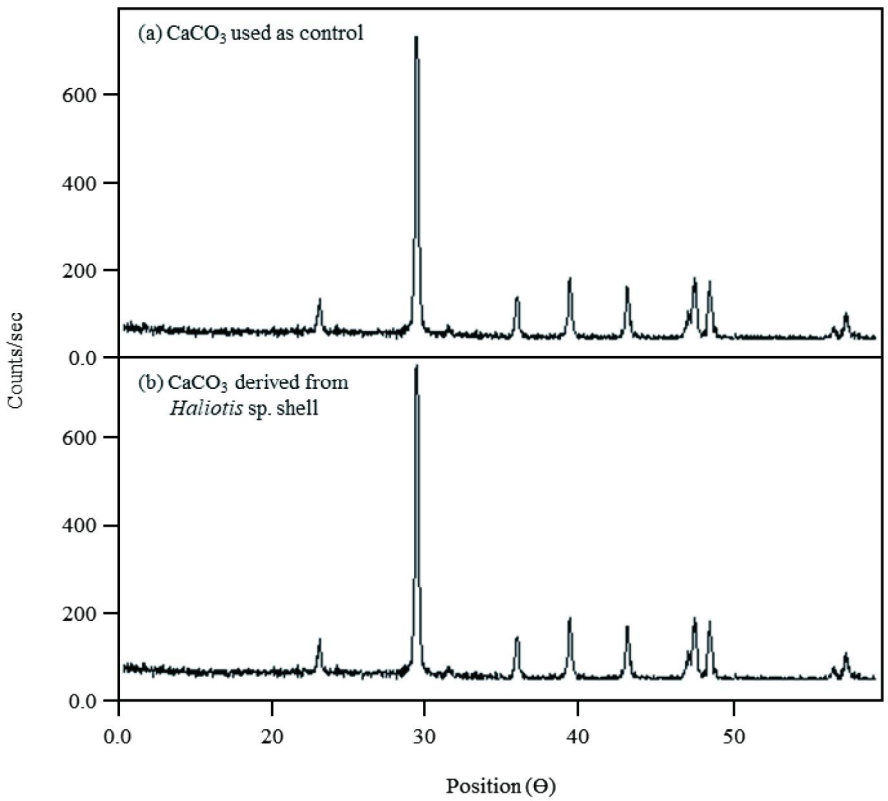

Fig. 9. XRD analysis of $CaCO_3$ synthesized from *Haliotis* sp. shell-derived CaO by the infusion of CO_2. (a) Peaks of control $CaCO_3$ commercially purchased and (b) peaks of $CaCO_3$ derived from *Haliotis* sp. shells.

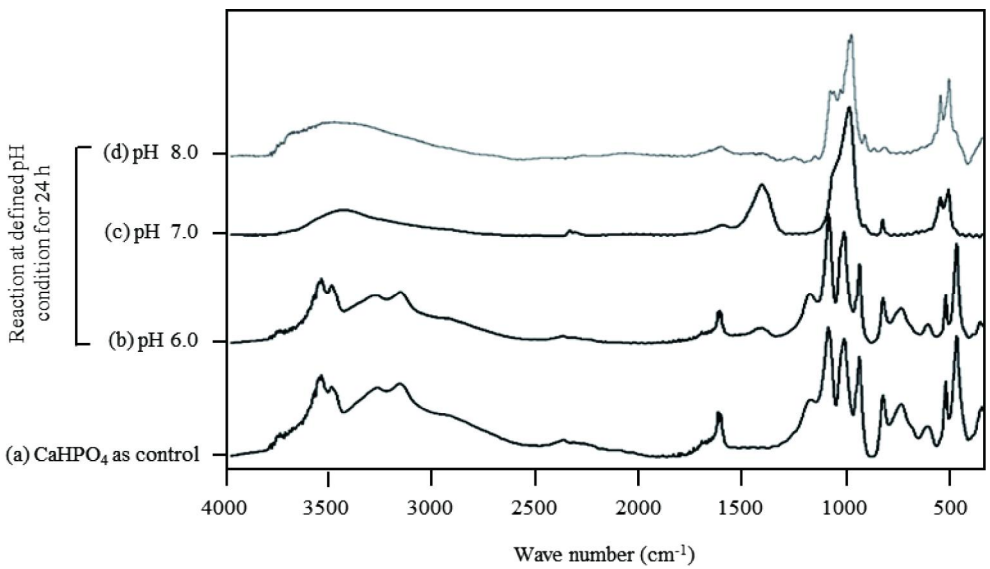

Fig. 10. FT-IR analysis of $CaHPO_4$ synthesized from *Haliotis* sp. shell-derived $CaCO_3$ by a chemical reaction. (a) Spectrum of control $CaHPO_4$ commercially purchased and spectra of $CaHPO_4$ at a pH of (b) 6.0, (c) 7.0, and (d) 8.0 condition for 24 h, respectively.

1653 cm^{-1}. The absorption peaks at 1219 and 1134 cm^{-1} are attributed by (P=O)-associated stretching vibrations. The absorption at 1057 cm^{-1} is caused by P=O stretching vibrations. P-O-P asymmetric stretching vibrations lead to absorption peaks at 987, 876, and 791 cm^{-1}. These are well-known characteristic peaks of $CaHPO_4$ [45-47]. The reaction pH between H_3PO_4 and $CaCO_3$ is a critical factor in $CaHPO_4$ synthesis. As shown in Fig. 10(c) and (d), the peak positions of the ceramic products synthesized at pH values of 7.0 or 8.0 were different from the characteristic peaks of dicalcium phosphate dehydrate, which was used as the control. On the other hand, the positions of the peaks of the ceramic products synthesized at pH 6.0 matched the characteristic peaks of $CaHPO_4$, as shown in Fig. 10(b). These data indicate that the optimal pH for the synthesis of $CaHPO_4$ by the reaction of H_3PO_4 and Haliotis sp. shell-derived $CaCO_3$ is 6.0. XRD analysis was conducted to verify $CaHPO_4$ synthesis under the optimized conditions. The XRD spectrum of commercial $CaHPO_4$ used as a control showed characteristic diffraction peaks at 11.5°, 20.7°, 23.2°, 29.3°, and 31.4°, as shown in Fig. 11(a). Moreover, the XRD pattern of $CaHPO_4$ derived from Haliotis sp. shells matched the XRD pattern of commercial $CaHPO_4$, as shown in Fig. 11(b). Therefore, it can be concluded that $CaHPO_4$ was successfully synthesized via a reaction between H_3PO_4 and *Haliotis* sp. shell-derived $CaCO_3$ at pH 6.0.

Ⅲ-A-4. FT-IR and XRD characterization of β-TCP from $CaHPO_4$ synthesized from *Haliotis* sp. shell

β-TCP was synthesized by sintering a mixture composed of CaO and $CaHPO_4$ derived from *Haliotis* sp. shells. To determine the optimal conditions for β-TCP synthesis, sintering was performed at 950, 1000, 1050, and 1100℃ for 3 h. Later, the chemical properties of the synthesized composites were analyzed using FT-IR and XRD. As shown in Fig. 12(a), β-TCP used as the control could be easily identified by a broad band between 900 and 1200 cm^{-1} and by the presence of a peak

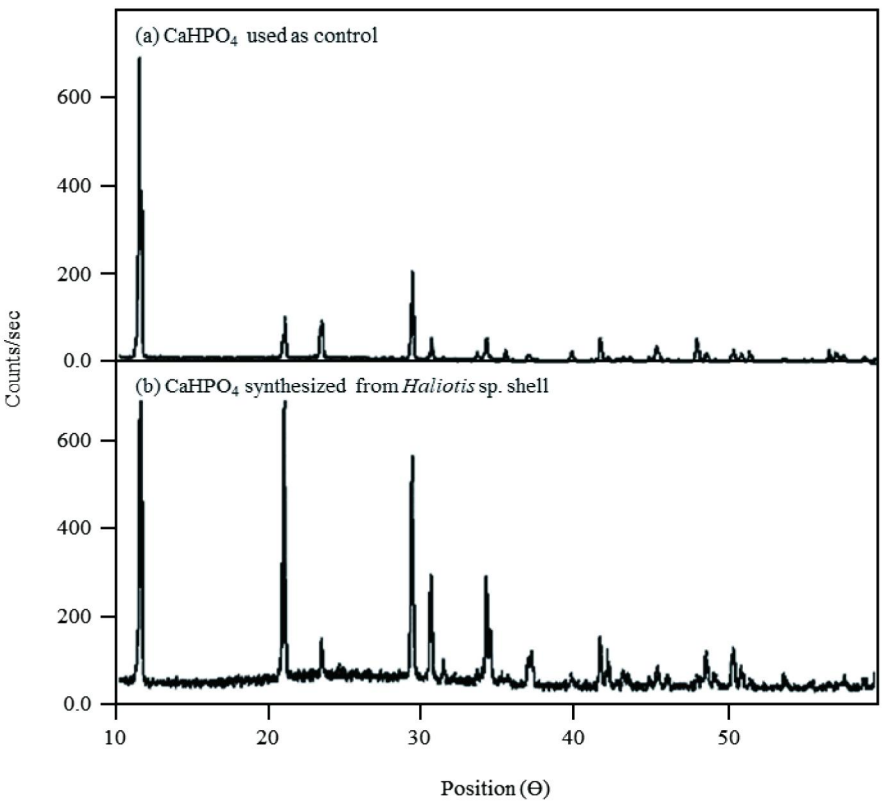

Fig. 11. XRD analysis of $CaHPO_4$ synthesized from *Haliotis* sp. shell-derived $CaCO_3$ by a chemical reaction. (a) Peaks of control $CaHPO_4$ commercially purchased and (b) peaks of $CaHPO_4$ synthesized by a chemical reaction between H_3PO_4 and *Haliotis* sp. shell-derived $CaCO_3$ at pH 6.0.

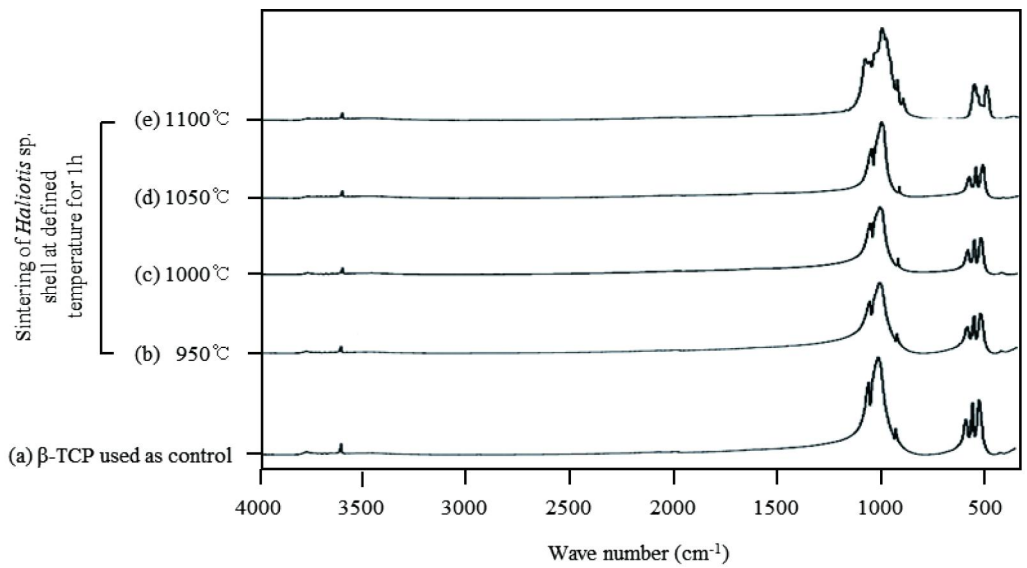

Fig. 12. FT-IR analysis of β-TCP synthesized from *Haliotis* sp. shell-derived $CaHPO_4$ by a chemical reaction. (a) Spectrum of control β-TCP commercially purchased and spectra of β-TCP sintered at (b) 950, (c) 1000, (d) 1050, and (3) 1100℃ for 3 h.

at 724 cm^{-1}. The peak at 1211 cm^{-1} is characteristic of non-degenerate deformation of hydrogen groups, such as H-OPO_3, O-PO_3, and HPO_4^{2-}. However, the absence of a band at 460 cm^{-1}, which is characteristic of α-TCP, is indicative of β-TCP [48]. As shown in Fig. 12 (b)-(d), the peak positions of the composites synthesized at 950 - 1050℃ matched the peak positions of β-TCP, which was used as the control. These results indicated that β-TCP was successfully synthesized by sintering a mixture of CaO and $CaHPO_4$ derived from *Haliotis* sp. shells at 950-1050℃. However, the peak positions of the composites synthesized at 1100℃ were different from the peak positions of the β-TCP control [Fig. 12(e)]. Taken together, these results indicate that the optimal sintering conditions for synthesizing β-TCP from a mixture of CaO and $CaHPO_4$ derived from *Haliotis* sp. shells include a sintering temperature of 950 - 1050℃ and sintering time of 3 h. XRD was also conducted to verify the synthesis of β-TCP under the optimized sintering conditions. As shown in Fig. 13(a), the diffraction pattern of control β-TCP corresponded with the peaks of β-TCP or whitlockite. The diffraction pattern of β-TCP synthesized under optimized sintering conditions from a mixture of CaO and $CaHPO_4$ derived from *Haliotis* sp. shells matched the diffraction pattern of control β-TCP. Thus, β-TCP obtained from a mixture of *Haliotis* sp. shell-derived CaO and $CaHPO_4$ was successfully synthesized by sintering at 950 - 1050℃ for 3 h.

Ⅲ-A-5. FT-IR and XRD characterization of HA from synthesized from *Haliotis* sp. shell

CaO synthesized from abalone shells was phosphorylated using H_3PO_4 to synthesize HA. Later, the synthesized composites were sintered at 1230℃ for 3 h. To verify the synthesis of HA, FT-IR and XRD analyses were conducted, as shown in Fig. 14. The FT-IR spectrum of the composite sintered at 1230℃ was obtained in the wavenumber range of 500 - 4000 cm^{-1}, as shown in Fig. 14.

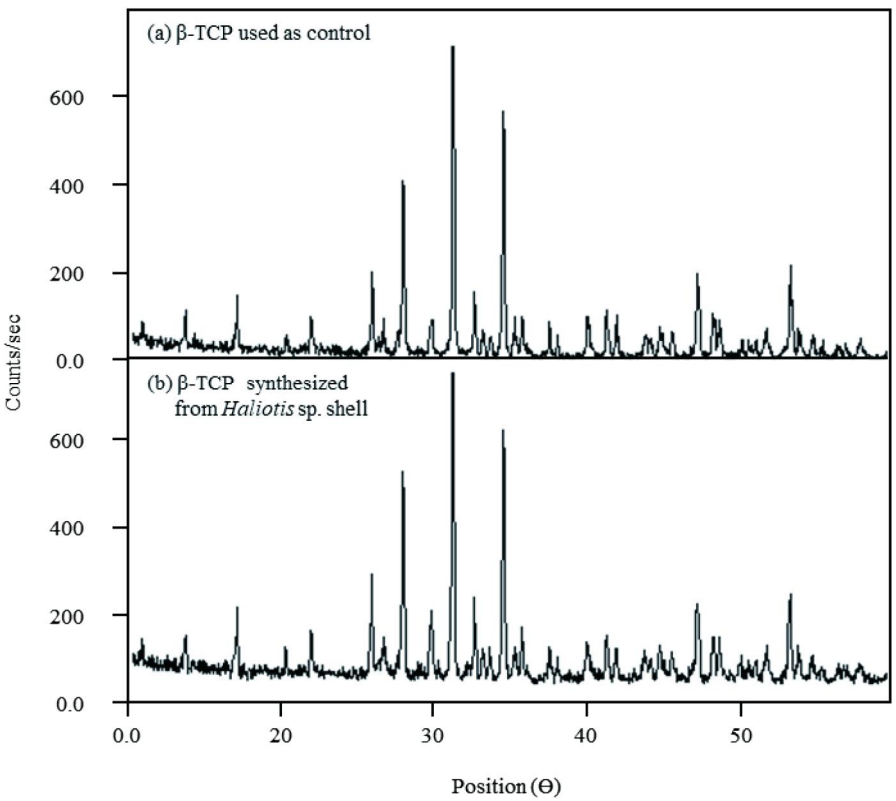

Fig. 13. XRD analysis of β-TCP synthesized from *Haliotis* sp. shell-derived $CaHPO_4$ by a chemical reaction. (a) Peaks of control β-TCP commercially purchased and (b) peaks of β-TCP sintered at 1050℃

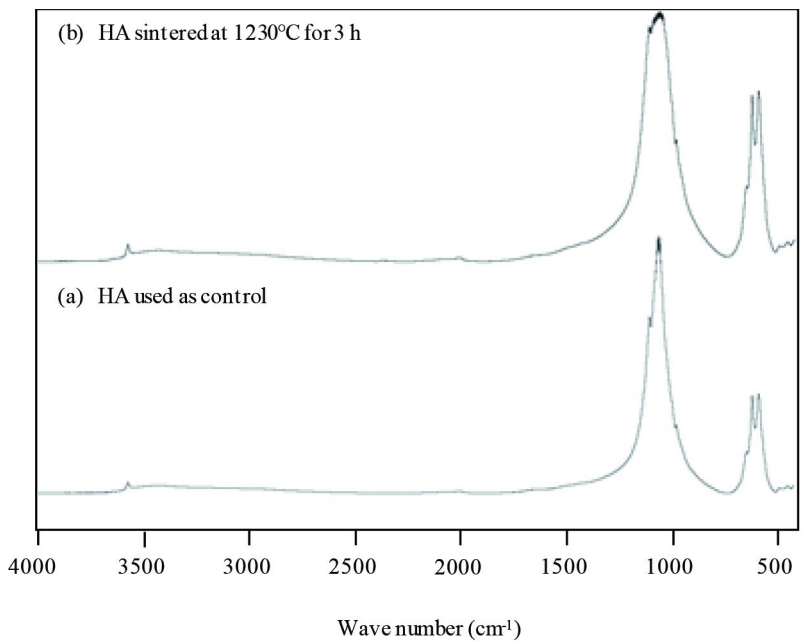

Fig. 14. FT-IR analysis to verify the optimal sintering temperature for the synthesis of HA. (a) Spectrum of control HA commercially purchased and (b) spectrum of HA derived from *Haliotis* sp. shell-derived CaO.

Especially, the peaks at 1030 and 570 cm^{-1}, which were attributed to PO_4^{3-}, indicated the presence of HA. The C-O vibrations in the CO_3^{2-} group disappeared and the spectrum obtained was characteristic of HA [49]. Furthermore, the XRD patterns of HA synthesized by sintering at 1230℃ and commercial HA are shown in Fig. 15. The XRD pattern of commercial HA used as the control showed characteristic peaks at 26°, 29°, 31.7°, 32.2°, 33°, 40°, 46.5°, 49°, and 53.2°. The XRD patterns of HA synthesized from *Haliotis* shells were similar [50]. Therefore, HA was synthesized successfully from *Haliotis* sp. shell-derived CaO by phosphorylation with phosphoric acid at pH 10.5 and sintering at 1230℃ for 3 h.

Ⅲ-A-6. FT-IR and XRD characterization of bone graft substitutes from synthesized from the *Haliotis* sp. shell

Bone graft substitutes were synthesized from a mixture of *Haliotis* sp. shell-derived HA and *Haliotis* sp. shell-derived β-TCP powders (at a ratio of 2 : 8). The chemical properties of the synthesized composites were analyzed using FT-IR and XRD. As shown in Fig. 16, the bone graft substitute used as a control is easily identified by a broad band between 566 and 603 cm^{-1} and by the presence of a peak at 940 - 1120 cm^{-1}. These peaks are characteristic of orthophosphates. Furthermore, as shown in Fig. 16, the broad absorption peaks at 631 and 3573 cm^{-1} result from O-H stretching vibrations. XRD was also performed to verify the synthesis of bone graft substitutes under the optimized sintering conditions. As shown in Fig. 17(a) and Fig. 17(b), the diffraction patterns of control β-TCP and HA correspond to the peaks of β-TCP and HA. The diffraction patterns of bone graft substitutes synthesized under optimized sintering conditions from a mixture of HA and β-TCP derived from *Haliotis* sp. shells matched the diffraction pattern of control bone graft substitutes. Thus, bone graft substitutes were successfully synthesized from a mixture of *Haliotis* sp. shell-derived HA and β-TCP by sintering at 1230℃ for 3 h.

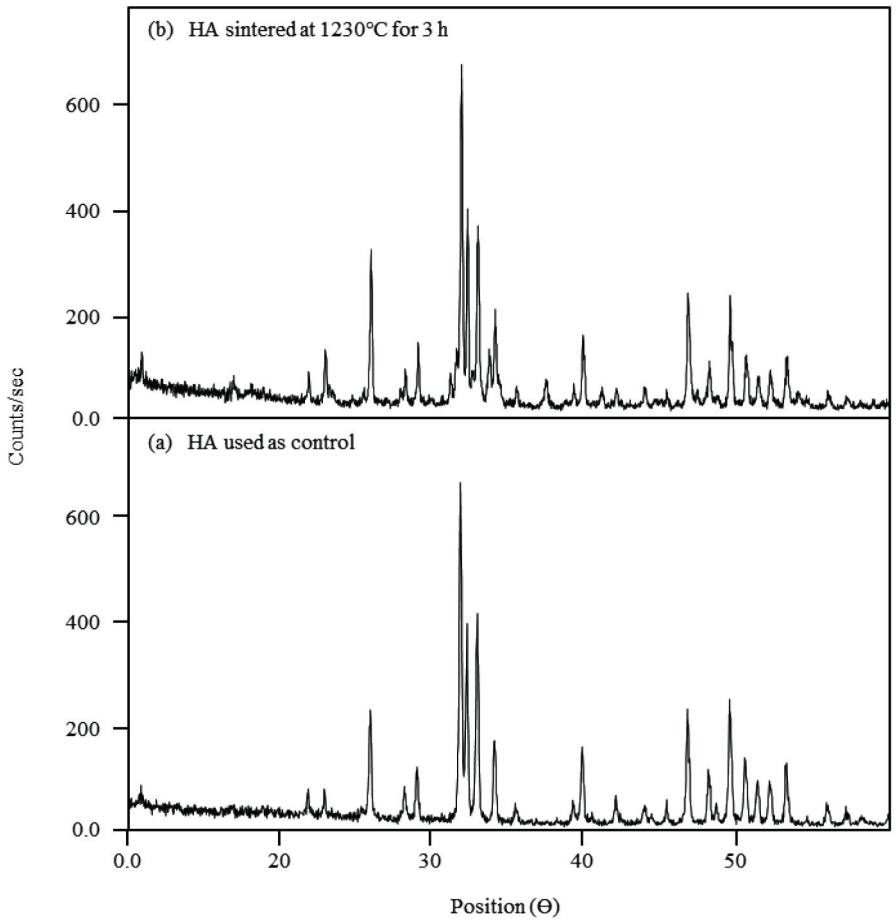

Fig. 15. XRD analysis to verify the optimal sintering temperature for the synthesis of HA. (a) Peaks of control HA commercially purchased and (b) peaks of HA sintered at 1230℃ for 3 h.

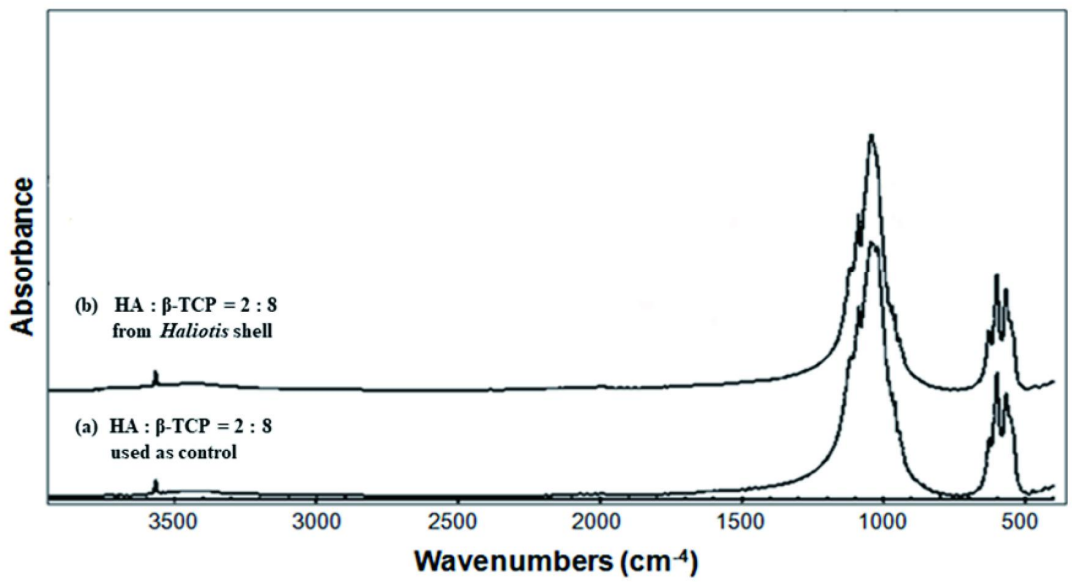

Fig. 16. Comparative analysis of the chemical compositions of bone grafting materials synthesized from a 2 : 8 mixture of HA and β-TCP. (a) Commercial bone graft substitutes composed of HA (20%) and β-TCP (80%) and (b) bone graft substitutes from *Haliotis* sp. shells composed of HA (20%) and β-TCP.

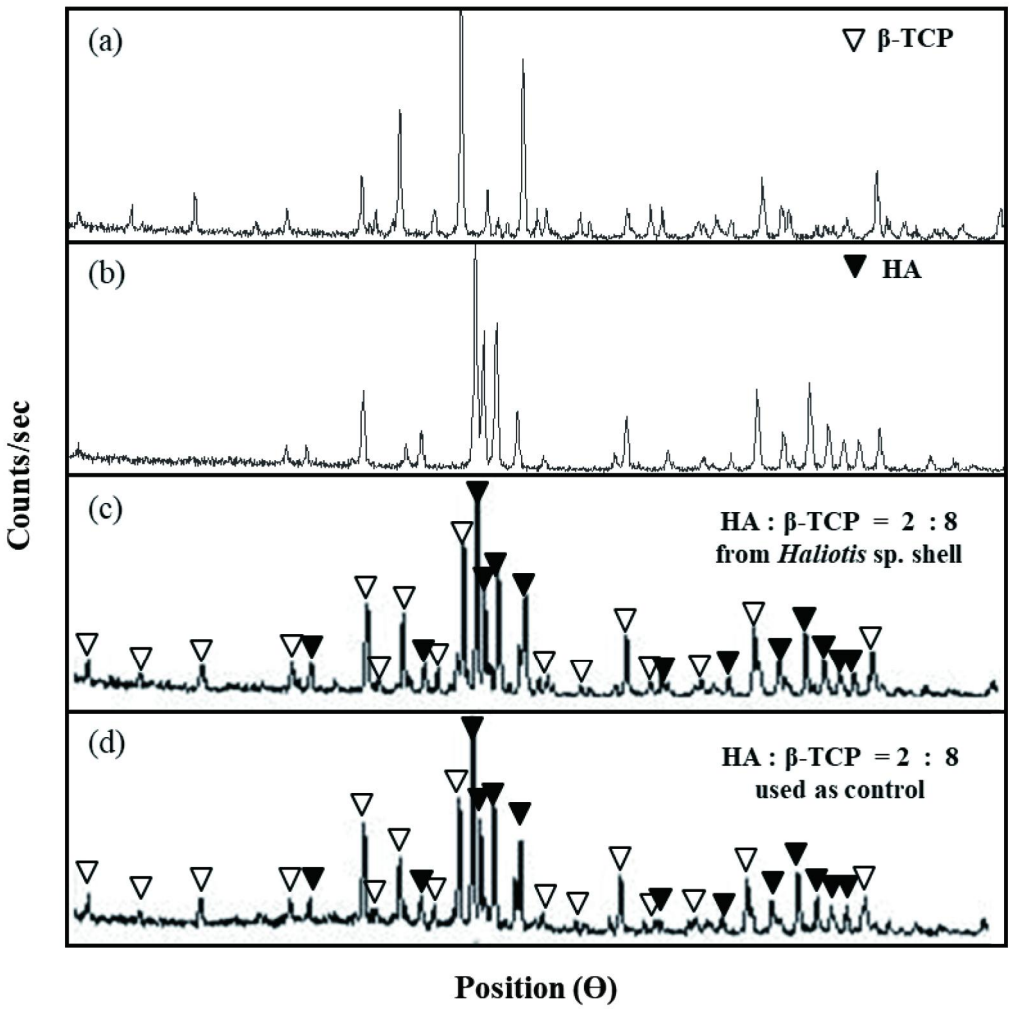

Fig. 17. XRD crystalline analysis of the bone grafting materials synthesized form a 2 : 8 mixture of HA and β-TCP. (a), β-TCP, (b), HA, (c) bone graft substitutes from the *Haliotis* sp. shells composed of HA (20%) and β-TCP, and (d) commercial bone graft substitutes composed of HA (20%) and β-TCP (80%).

Ⅲ-B. Evaluation of physical and chemical properties

Ⅲ-B-1. SEM and EDS mapping analysis of the bone graft substitutes from synthesized from the *Haliotis* sp. shell

The surface morphology and crystal size of each of the bone graft substitutes synthesized from mixtures of HA and β-TCP were studied using a SEM at an accelerating voltage of 5.5 kV. In Fig. 18, the sizes and shapes of the bone graft substitutes are shown at a magnification of 100X, the surface roughness values of the bone grafting materials are shown at magnifications of 500X and 1500X, and the macroporosities and pore structures are shown at a magnification of 5000X. As shown in Fig. 18, micropores of 10 - 100 μm diameter were found on both the internal and external surfaces of all the bone grafting substitutes synthesized from mixtures of HA and β-TCP. As shown in Fig. 19, the Ca/P ratio of the bone grafting substitutes synthesized from the *Haliotis* sp. shells by mixing HA and β-TCP at a ratio of 2 : 8 is 1.64, which is similar to the Ca/P ratio of bone tissue isolated from a human body.

Ⅲ-B-2. pH value of the bone graft substitutes from synthesized from *Haliotis* sp. shell

The pH values of the eluate from the each bone grafting substitutes prepared according to the guidelines provided by MFDS, Republic of Korea, were measured using a pH meter and qualitatively using a pH paper. As shown in Fig. 20, all the bone grafting substitutes synthesized using mixtures of HA and β-TCP exhibited pH values in the range of 8.6 - 8.8, which were similar to the physiological pH value.

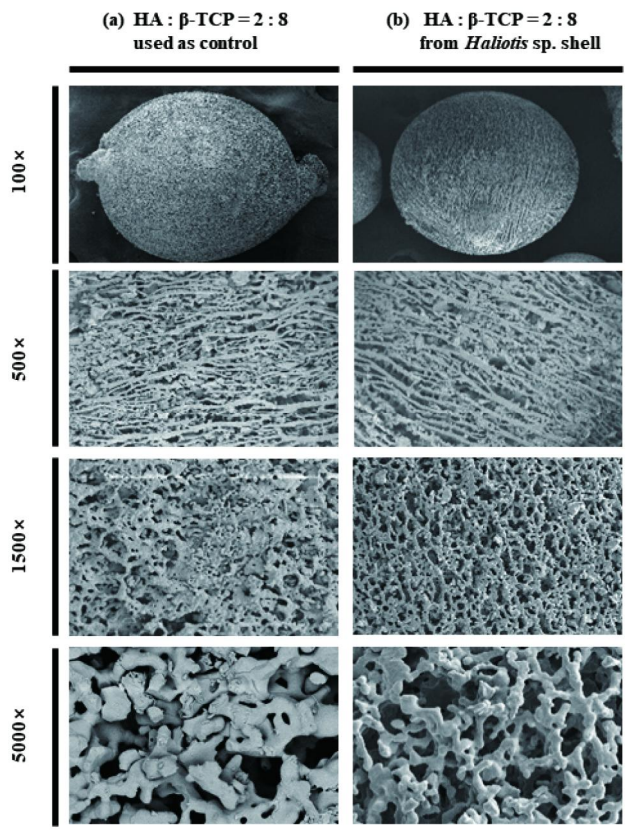

Fig. 18. SEM evaluation of the surface morphology, roughness, and pore size of the bone grafting substitutes synthesized from a 2 : 8 mixture of HA and β-TCP synthesized from *Haliotis* sp. shells. (a) Commercial bone graft substitutes composed of HA (20%) and β-TCP (80%) and (b) bone graft substitutes from the *Haliotis* sp. shells composed of HA (20%) and β-TCP.

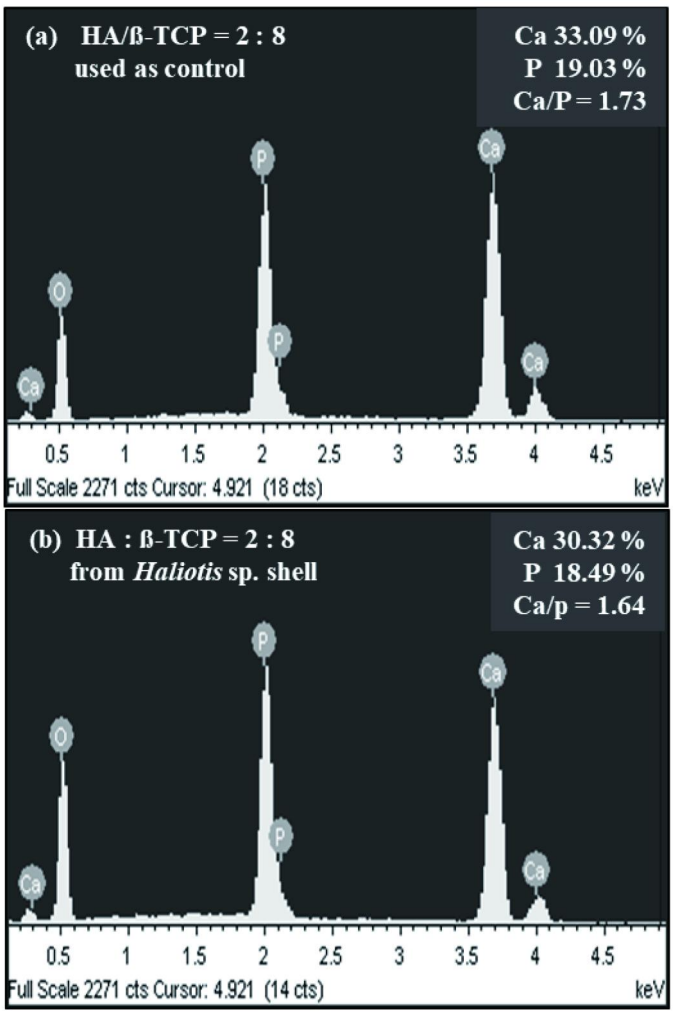

Fig. 19. Ca/P compositions of the bone grafting materials synthesized from a 2 : 8 mixture of HA and β-TCP synthesized from *Haliotis* sp. shells. (a) Commercial bone graft substitutes composed of HA (20%) and β-TCP (80%) and (b) bone graft substitutes from *Haliotis* sp. shells composed of HA (20%) and β-TCP.

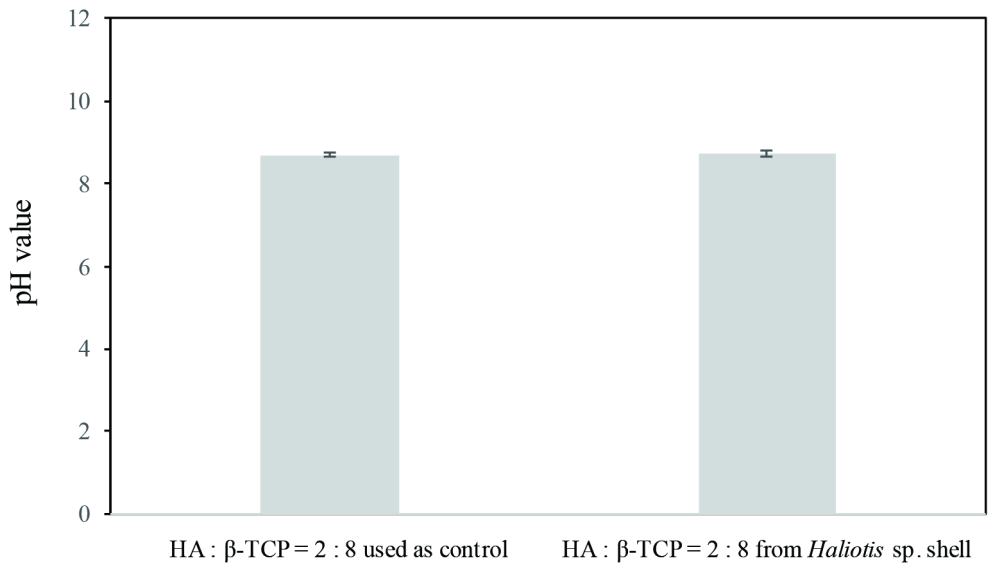

Fig. 20. pH values of the bone grafting materials synthesized from a 2 : 8 mixture of HA and β-TCP synthesized from *Haliotis* sp. shells. The pH values of effluents of each bone grafting substitutes prepared by following the guide lines provided by MFDS, were measured by pH meter.

Ⅲ-B-3. Dissolution and wettability test of the bone graft substitutes from synthesized from the *Haliotis* sp. shell

The solubilities of the bone grafting materials synthesized from mixtures of HA and β-TCP were measured using a protocol provided by MFDS, Republic of Korea. As shown in Fig. 21, the bone graft substitutes synthesized at a 2 : 8 mixing ratio of HA and β-TCP from *Haliotis* sp. shells might have a better stability than the control bone grafting substitutes.

The wettability of the bone grafting substitutes synthesized using mixtures of HA and β-TCP was measured using a protocol provided by MFDS, Republic of Korea. Briefly, 0.5 g of each synthesized bone grafting substitute was immersed with 1 mL of distilled water at room temperature for 30 min. After reaction, the remaining volume of the distilled water was measured using a microbalance. As shown in Table 2, the wettability of a bone graft substitute does not have a direct influence on its performance. However, in a clinical setting, when a graft is placed, the graft material implanted into the bone can absorb some amount of blood and the graft can be located in the bone defect region.

Ⅲ-C. *In vitro* cytocompatibility

Ⅲ-C-1. Cell cytotoxicity of *Haliotis* sp. shell-derived bone graft substitutes

To analyze the cell cytotoxicity of effluent prepared from *Haliotis* sp. shell-derived bone graft substitutes, they were used to treat MG-63 cells. As shown in Fig. 22, the

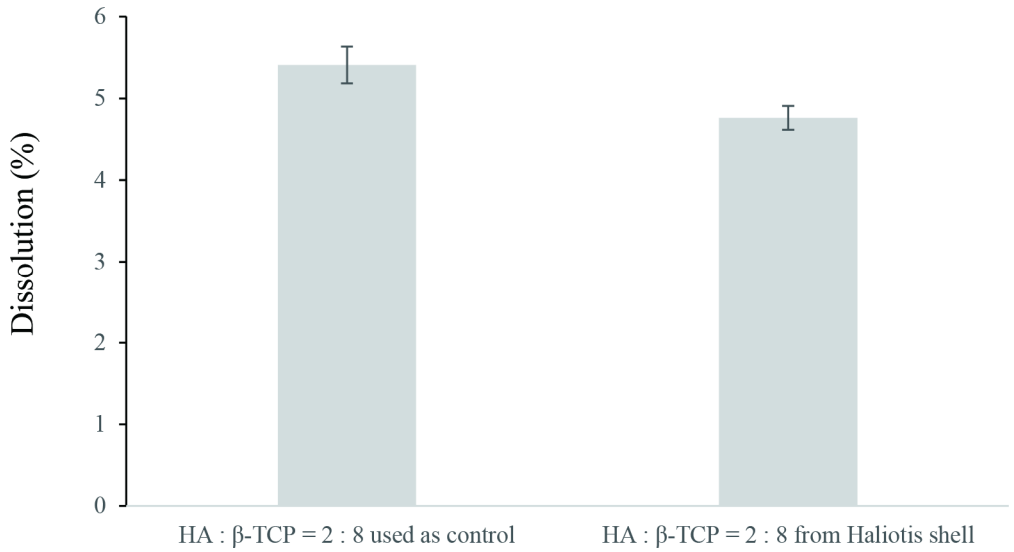

Fig. 21. Solubilities of the bone grafting materials synthesized from a 2 : 8 mixture of HA and β-TCP. The solubility of bone grafting substitutes was measured by the protocol provided by MFDS, Republic of Korea.

Table 2. Wettability of the bone grafting substitutes synthesized from a 2 : 8 mixture of HA and β-TCP.

	HA : β-TCP = 2 : 8 used as control					HA : β-TCP = 2 : 8 from Haliotis shell				
Bone graft	0.1050	0.1045	0.1048	0.1006	0.1026	0.1000	0.1020	0.1006	0.1015	0.1037
Before dropping	1.1700	1.1650	1.1800	1.1605	1.1689	1.1530	1.1630	1.1545	1.1650	1.1675
After suction	1.2850	1.2810	1.2930	1.2520	1.2789	1.2590	1.2690	1.2600	1.2680	1.2790
Difference	0.1150	0.1160	0.1130	0.0915	0.1100	0.1060	0.1060	0.1060	0.1030	0.1115
Ratio	91.30	99.09	92.74	90.95	93.27	94.34	96.23	94.90	98.54	93.00
Average(Rm)	91.67%					95.40%				
Standard deviation (Rs)	1.31					1.88				

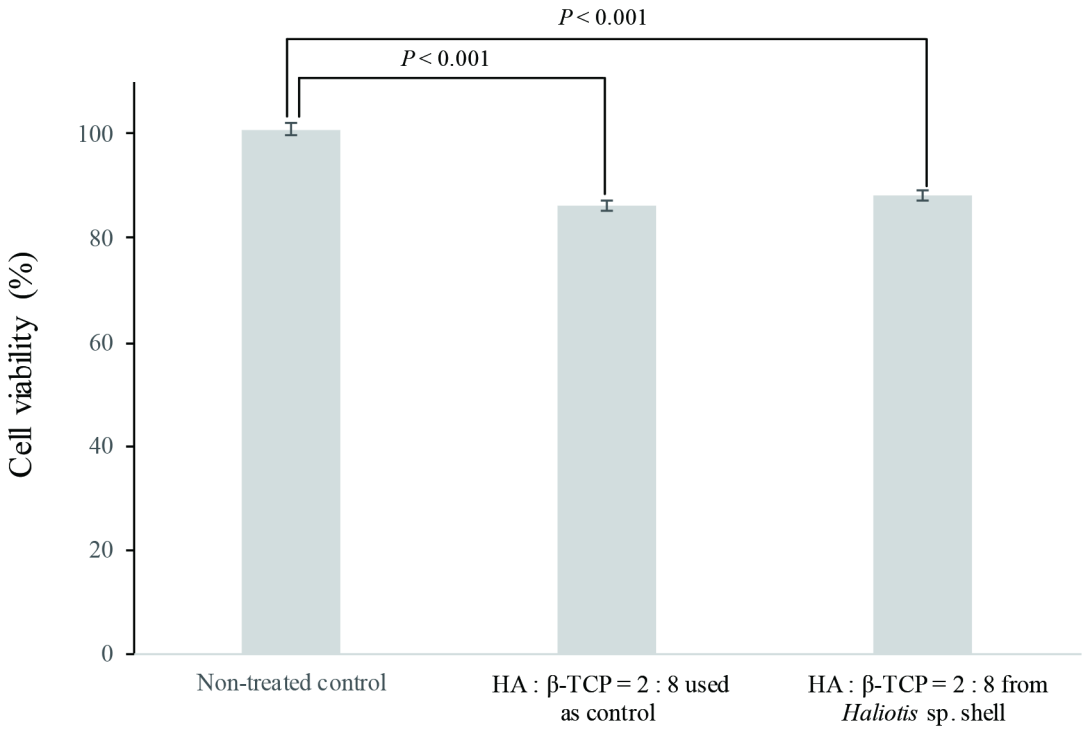

Fig. 22. Cell cytotoxicity of the bone grafting substitutes synthesized from a 2 : 8 mixture of HA and β-TCP synthesized from *Haliotis* sp. shells. Cell cytotoxicity of the bone grafting materials was evaluated by MTT assay on MG-63 cells; the results are shown in the form of mean ± standard deviation (SD) of three samples. The standard errors are shown as error bars ($P < 0.001$).

relative cytotoxicity of *Haliotis* sp. shell-derived bone graft substitutes and commercial bone graft substitutes were estimated to be 86.36% ± 0.95% and 88.1% ± 0.99%, respectively, as compared to the control. Although the relative cytotoxicity of *Haliotis* sp. shell-derived bone graft substitutes is less than that of commercial bone graft substitutes, it was not significant.

Ⅲ-C-2. Cell viability of *Haliotis* sp. shell-derived bone graft substitutes

To verify apoptotic cell death in MG-63 cells treated with the effluent prepared from *Haliotis* sp. shell-derived bone graft substitutes, DAPI staining was performed to observe the cells with nuclear condensation. As shown in Fig. 23, cells with nuclear condensation could not be observed in the MG-63 cells treated with the effluents prepared from the two bone graft substitutes. Moreover, a live-and-dead cell viability assay was performed to determine the number of live and dead cells attached to the bone graft substitutes and *Haliotis* sp. shell-derived bone graft substitutes. The live cells exhibited green fluorescence owing to green calcein AM and the dead cells were stained in red with ethidium homodimer-1; the live and dead cells were visualized and counted under an inverted fluorescent microscope. As shown in Fig. 23, MG-63 cells in the presence of either commercial or *Haliotis* sp. shell-derived bone graft substitutes were stained with green fluorescence via the cleavage of membrane-permeable calcein AM by cytosolic esterase present in living cells. Furthermore, dead cells with red fluorescence due to ethidium homodimer-1 staining were not observed in the MG-63 cell population cultured with the *Haliotis* sp. shell-derived bone graft substitutes for 24 h. This suggests that the *Haliotis* sp. shell-derived bone graft substitutes exhibit an excellent biocompatibility as bone grafting materials.

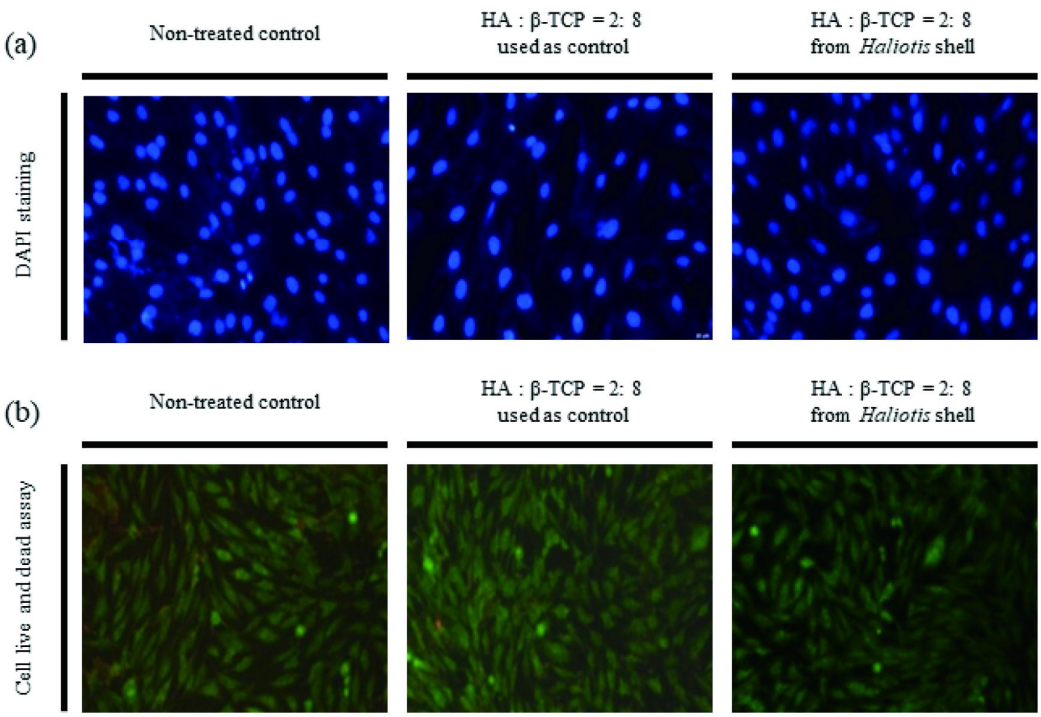

Fig. 23. Comparison of cell survival with bone grafting substitutes synthesized from a 2 : 8 mixture of HA and β-TCP synthesized from *Haliotis* sp. shells. Cell survival was analyzed by nuclear staining using (a) DAPI and (b) live-and-dead assay. Live cells were stained as green by green calcein AM and dead cells were stained as red by ethidium homodimer[-1].

Ⅲ-C-3. Osteoconductivity of *Haliotis* sp. shell-derived bone graft substitutes in MG-63 cells

To evaluate the osteoconductivity of *Haliotis* sp. shell-derived bone graft substitutes, MG-63 cells were cultured with *Haliotis* sp. shell-derived bone graft substitutes for 4, 7, and 11 days and the resultant mineralization was evaluated using Alizarin Red S staining. As shown in Fig. 24, mineralized nodules were observed in MG-63 cells cultured over 7 and 11 days with both control and *Haliotis* sp. shell-derived bone graft substitutes. Although the level of mineralization in MG-63 cells cultured with *Haliotis* sp. shell-derived bone graft substitutes was similar to that obtained with commercial substitutes, these are suggesting that osteoconductivity of the *Haliotis* sp. shell-derived bone graft substitutes are at least similar to used as control one.

Ⅲ-D. *In vivo* Osteoconductivity

Ⅲ-D-1. Radiographic evaluation of bone regeneration in animal model with calvarial bone defection

To evaluate the biological safety and osteoconductivity of the synthesized bone graft substitutes, as shown in Fig. 25, 8-mm calvarial bone defects were produced on experimental animals according to the protocol approved by the IACUC at Chosun University, Gwangju, Republic of Korea. Subsequently, the synthesized bone graft substitutes were transplanted onto the bone defect regions of the experimental animals.

Eight weeks after the transplantation of the bone graft substitutes, the calvarial bones were collected to evaluate the ability of bone graft substitutes as bone graft

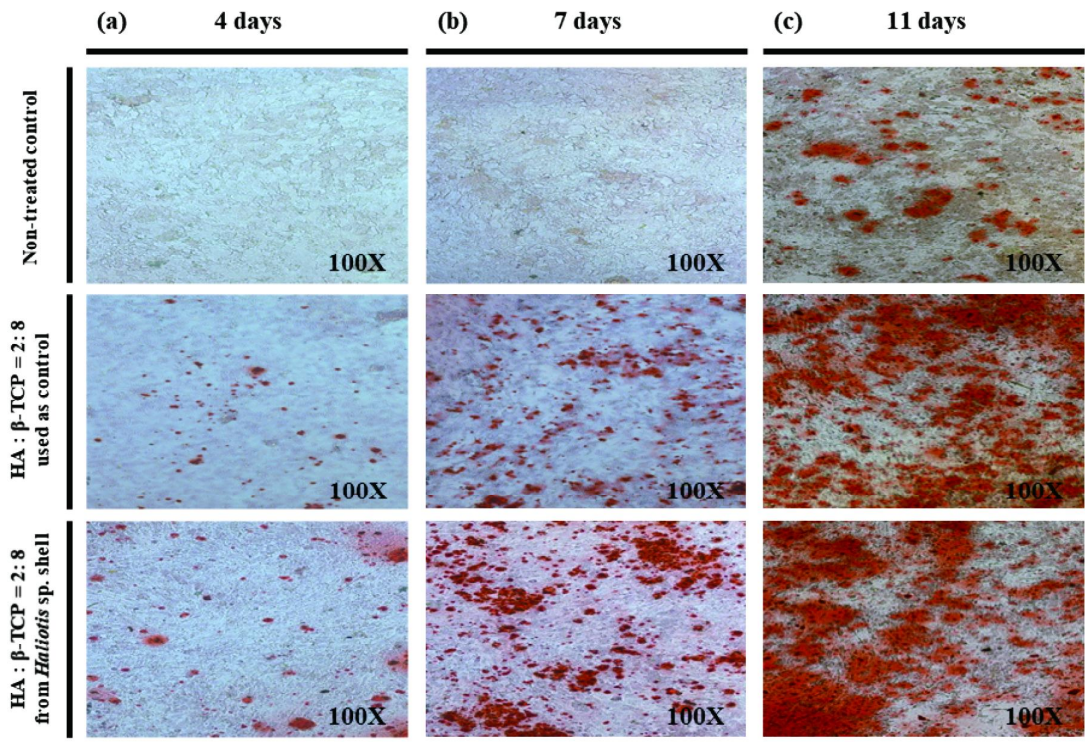

Fig. 24. Osteoconductivity of *Haliotis* sp. shell-derived bone graft substitutes in MG-63 cells. MG-63 cells were cultured with the controls and *Haliotis* sp. shell-derived HA for 4, 7, and 11 days. Osteoconductivity was observed by the Alizarin Red stain and was verified by the optical microscopy at 100X magnification after (a) 4 days, (b) 7 days, and (c) 11 days.

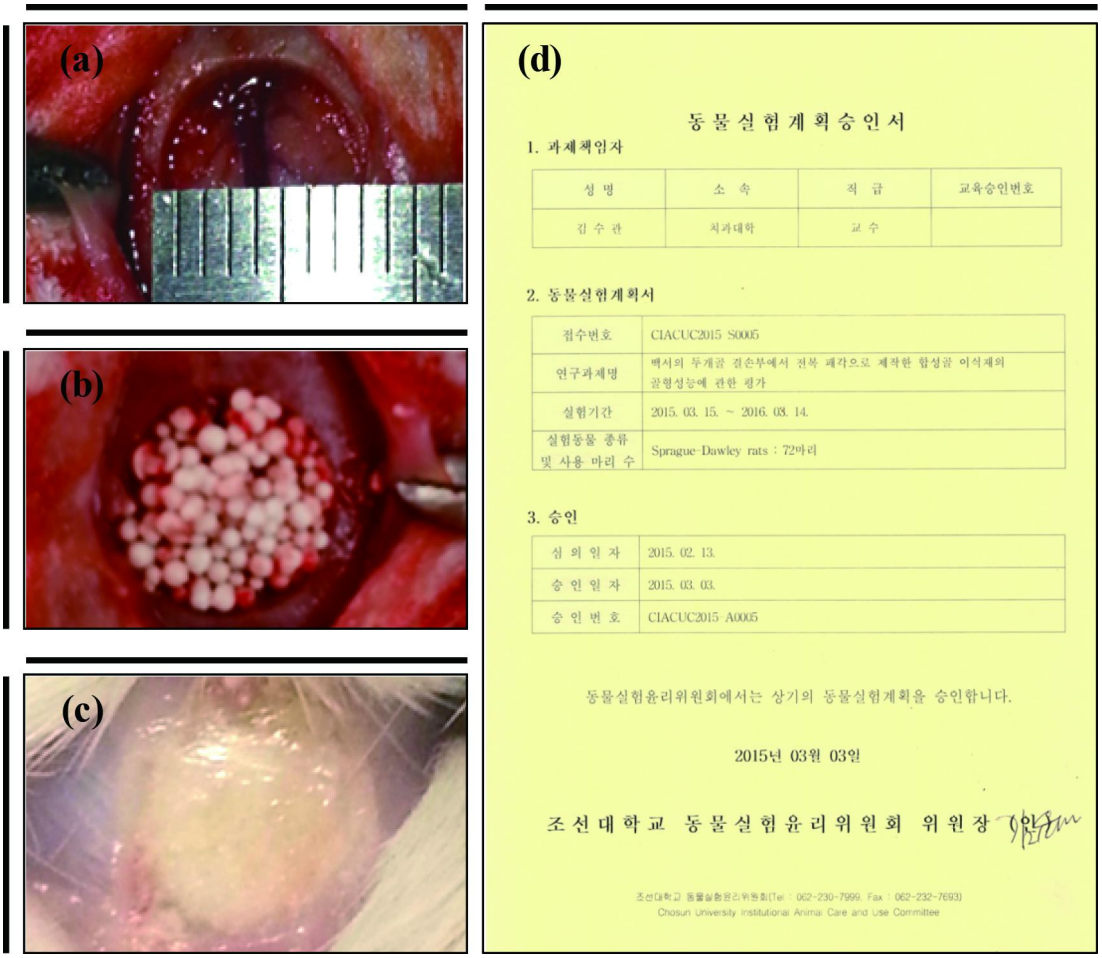

Fig. 25. Rat calvarial critical-size (8 mm) osteotomy defect surgery procedure. (a) 8-mm critical-size defects were formed using an 8-mm trephine bur. (b) Synthesized bone graft substitutes were placed in the defect area. (c) Defect area at 8 weeks after the transplantation of bone graft substitutes Rat calvarial critical-size (8 mm) osteotomy defect surgery Procedure. (d) approved by IACUC at Chosun Universitym Gwanju republic of Korea.

materials by radiographic analysis using X-ray and micro-CT techniques. As shown in Fig. 26, bone defects could still be observed in the defect region of the calvarial bone when it was not transplanted with a bone graft substitute. Furthermore, radiographic observations revealed that bone graft substitutes transplanted on the defect regions induced significant bone formation. Hence, both visual inspection and radiographic analysis clearly indicated that the synthesized bone graft substitutes exhibit excellent osteoconductivity.

Ⅲ-D-2. Histological evaluation of bone regeneration in animal model with calvarial bone defection

To evaluate the osteoconductivity of the synthesized bone graft substitutes from *Haliotis* sp. shells, harvested calvarial bones were decalcified and histological analysis was conducted using H&E staining to observe the morphological changes in tissues. Safranin-O and fast green staining were conducted to verify new bone formation at the defect regions in the experimental animals. As shown in Fig. 27, the results of H&E staining showed that the transplants affected only the morphology but did not induce inflammation in the defect regions of the experimental animals. Furthermore, to evaluate new bone formation in the defect regions transplanted with synthesized bone graft substitutes from *Haliotis* sp. shells, safranin-O & fast green staining was performed as shown in Fig. 28. Similar to the results of radiographic analysis, the safranin-O & fast green staining results revealed the formation of new bones under the transplanted bone graft substitutes from *Haliotis* sp. shells. Therefore, taken together, these results clearly suggest that the bone graft substitutes substituted from *Haliotis* sp. shells exert potent physio-chemical activities as bone graft materials.

(a)

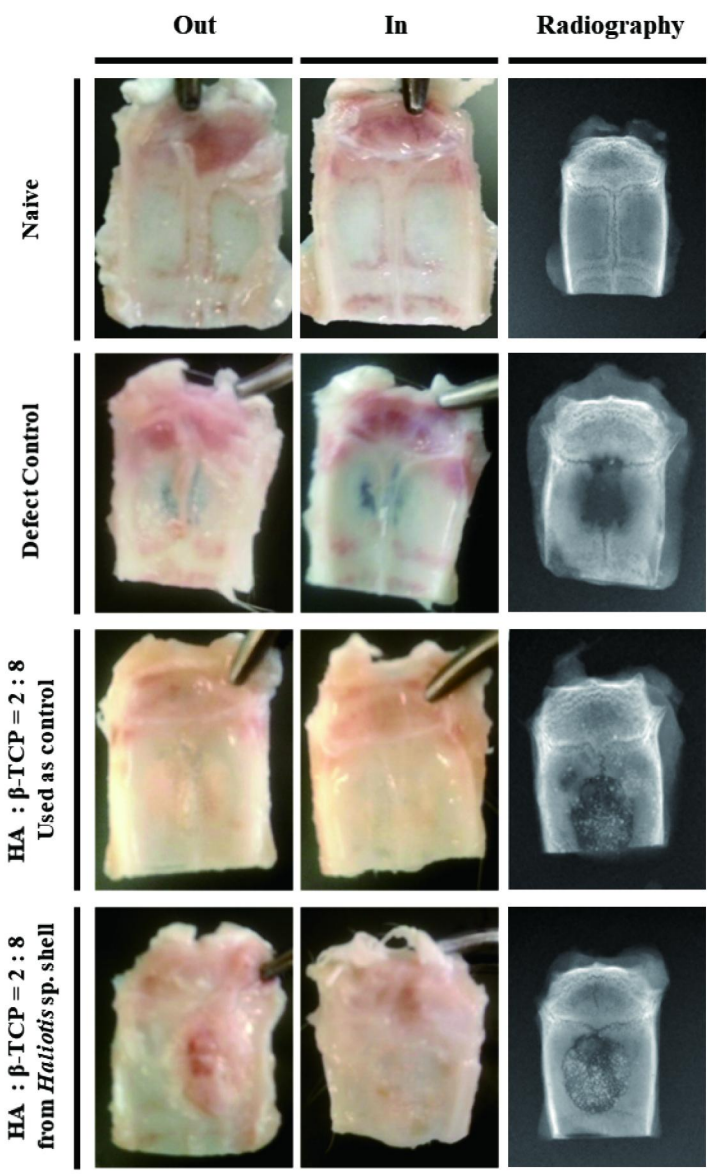

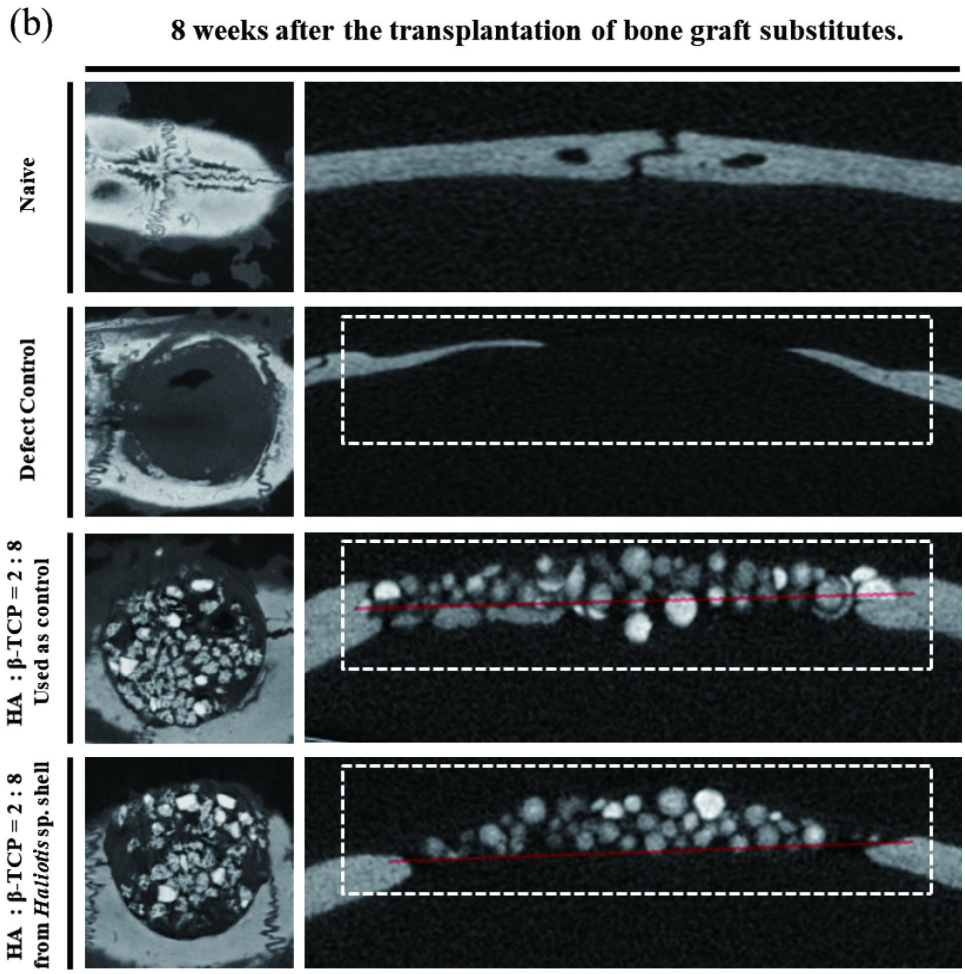

Fig. 26. Radiographic evaluation of the defect area at 8 weeks after the transplantation of bone graft substitutes using the X-ray and Micro-CT images analysis. After 8 weeks post-transplantation of bone graft substitutes in the defect areas of animal models, tissues were harvested and immediately fixed using 4% paraformaldehyde for 4 days. After fixation, the tissues were subjected to X-ray and micro-CT analysis to evaluate bone regeneration at the defect regions. (a) Photographs and X-ray observations of the rat calvarial defects post-bone grafting. (b) Micro-CT images of bone regeneration 8 weeks after bone grafting.

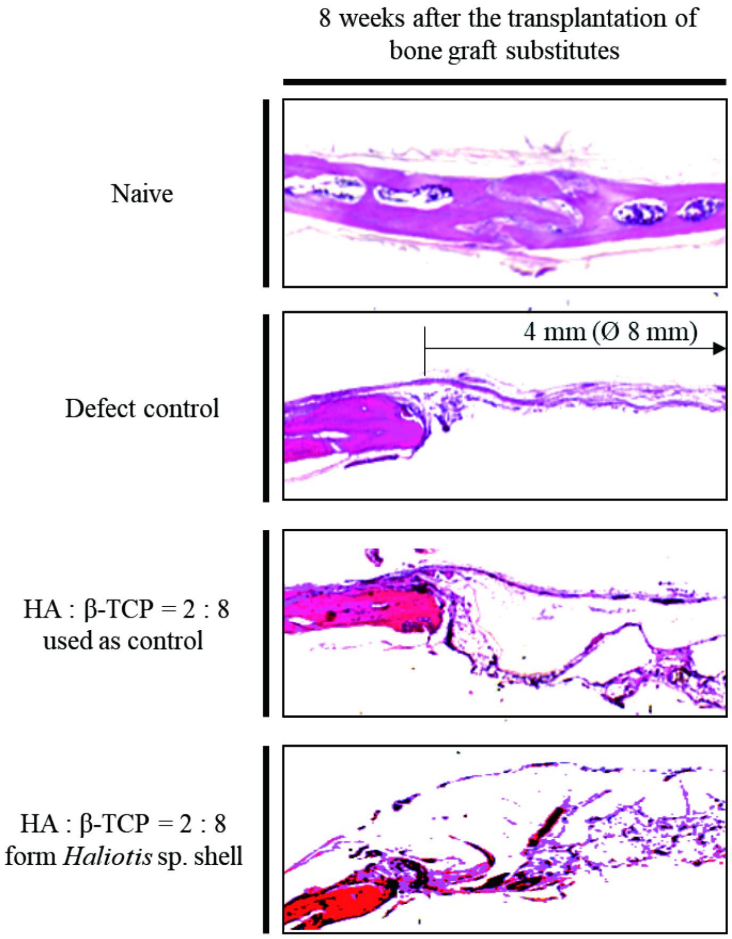

Fig. 27. The histological evaluation of defecting sites at 8 weeks after transplantation of synthetic bone grafting substitutes. Experimental animals were sacificed at 8 weeks post-surgery. The collected bone sections were observed by histological analysis using the H&E staining.

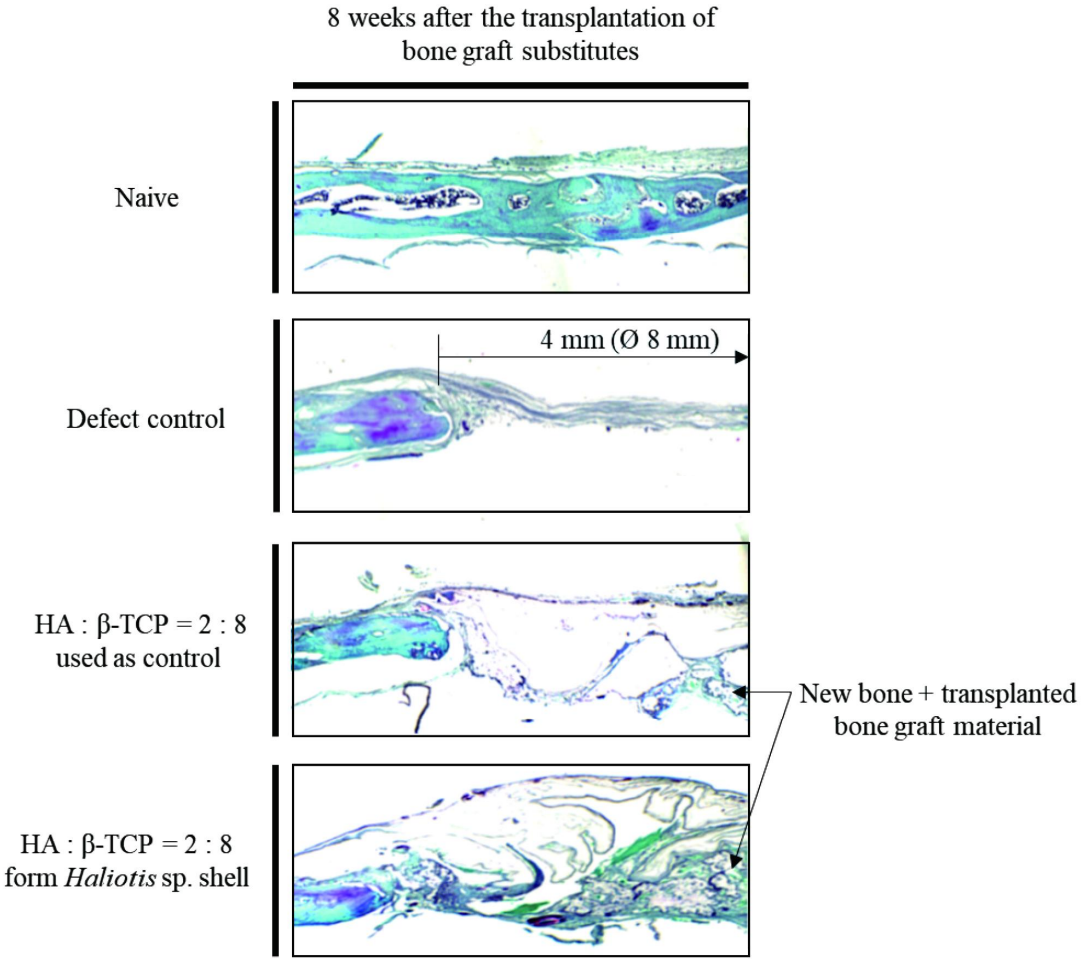

Fig. 28. The histological evaluation of defecting sites at 8 weeks after transplantation of synthetic bone grafting substitutes. Experimental animals were sacificed at 8 weeks post-surgery. The collected bones were evaluated by histological analysis using safranin-O & fast green staining.

Ⅳ. Discussion

GBR is frequently performed to regenerate bones for implant replacement in dental surgery; this usually requires bone grafting materials to promote bone healing [51]. The importance of bone grafting materials in GBR has been reported in numerous studies. Bone grafting materials are routinely used to reconstruct bone defects caused by trauma, accident, or infections in oral and orthopedic surgery. Although autologous bone grafting materials are often preferred for bone regeneration, they are harvested from elsewhere in the body (e.g., autologous iliac crest or mandibular symphysis) [52]. To overcome this drawback, biomaterials, such as calcium phosphate bioceramics, zirconia, and bio-glass, are being developed as bone substitutes [52-55].

β-TCP and HA are partially resorbable bone substitutes characterized by biocompatibility, osteoconductivity, and osteoinductivity. Calcium phosphate-based β-TCP and HA biomaterials have been successfully used for over 40 years as basic materials for replacing and promoting the reconstruction of damaged or defective hard tissue. Although β-TCP and HA are commonly derived from inorganic sources, such as mineral rock, they can also be synthesized from natural materials containing calcite or aragonite, such as eggshells, cuttlefish bones, and oyster shells. *Haliotis* sp. shells are marine gastropods inhabiting East Asia; they are the most valued commercial edible sea snails in aquaculture [56, 57]. *Haliotis* sp. shell flesh is widely considered a desirable food in Korea, Japan, and China. Therefore, an increase in *Haliotis* sp. consumption is accompanied by an increase of "useless" shells, which are considered to be environmental pollutants. Although abalone shells are used as decorative items and as a material for jewelry, buttons, buckles, and inlay making, most of them are discarded by dumping into ocean. Therefore, an industrial-scale recycling process is needed to prevent marine pollution caused by such dumping of abalone shells. With this in mind, we aimed to synthesize β-TCP and HA from *Haliotis* sp. shells in the present study.

CaO is an important compound in the synthesis of bioceramics. *Haliotis* sp. shells were completely sintered at 900, 950, and 1000℃ to synthesize CaO. Thereafter, the physiochemical characteristics of composites synthesized at different sintering temperatures were analyzed by FT-IR and XRD. As shown in Fig. 6 and 7, the physiochemical characteristics of the composite synthesized by sintering at 950℃ were similar to those of commercial CaO, which was used as a control. As shown in Fig. 6, the FT-IR results revealed a sharp band at 3656 cm^{-1}, two broad weak bands centered at approximately 3822 and 3388 cm^{-1}, a medium doublet centered at around 1444 cm^{-1}, and a very strong absorption below 600 cm^{-1} for all the synthesized composites. Furthermore, it can be seen in Fig. 7 that commercial (control) CaO exhibited diffraction peaks at 32.24°, 37.4°, and 53.92°. The XRD pattern of CaO derived from abalone shells by sintering at 950℃ was similar to that of commercial CaO. These results indicate the high purity of CaO synthesized from abalone shells by sintering.

$CaHPO_4$ is generally synthesized by a chemical reaction between $CaCO_3$ and phosphoric acid. Hence, $CaCO_3$ is required to synthesize $CaHPO_4$, which is a precursor for TCP. As shown in Fig. 8, $CaCO_3$ was successfully synthesized by a chemical reaction between $Ca(OH)_2$ and CO_2. The FT-IR spectrum of commercial $CaCO_3$ (Fig. 8) used as the control included bands at 713, 875, and 1418 cm^{-1} corresponding to the asymmetrical stretching vibration peaks of O-C-O. These are well-known characteristic peaks of calcite [44, 58]. Moreover, $CaCO_3$ synthesized by the infusion of CO_2 gas into $Ca(OH)_2$ derived from *Haliotis* sp. shells exhibited similar bands. Meanwhile, the XRD pattern of commercial $CaCO_3$ (control) showed characteristic diffraction peaks at 23.09°, 29.40°, 36.0°, 39.43°, 43.18°, and 48.52° (Fig. 8), all of which indicate the formation of a calcite phase [45].

To obtain $CaHPO_4$, the synthesized $CaCO_3$ was reacted with phosphoric acid; the reaction pH is critical in this case. Therefore, $CaCO_3$ was reacted with phosphoric acid under various pH conditions. Each of the synthesized composites was compared with commercial $CaHPO_4$ by FT-IR. As shown in Fig. 10(a), the

broad absorption peak between 2400 to 3500 cm^{-1} results from O-H stretching vibrations. H-O-H bending leads to absorption at 1653 cm^{-1}. Absorptions at 1219 and 1134 cm^{-1} are caused by (P=O)-associated stretching vibrations, while the absorption at 1057 cm^{-1} is caused by P=O stretching vibrations. P-O-P asymmetric stretching leads to absorption at 987, 876, and 791 cm^{-1}. These are characteristic peaks of $CaHPO_4$ [45-47]. As shown in Fig. 10(c) and Fig. 10(d), the peak positions of the ceramic products synthesized at pH 7.0 or 8.0 were different from the characteristic peaks of dicalcium phosphate dehydrate, which was used as the control. On the other hand, the peak positions of the ceramic products synthesized at pH 6.0 matched the characteristic peaks of $CaHPO_4$, as shown in Fig. 10(b). These data indicate that the optimal pH for the synthesis of $CaHPO_4$ via chemical reaction between H_3PO_4 and *Haliotis* sp. shell-derived $CaCO_3$ is 6.0.

Subsequently, to verify the synthesis of $CaHPO_4$, the composite synthesized by the chemical reaction between $CaCO_3$ and phosphoric acid at pH 6.0 was compared with commercial $CaHPO_4$ by XRD. As shown in Fig. 11(b), the physiochemical characteristics of the composite synthesized at pH 6.0 were similar to the characteristics of commercial $CaHPO_4$. The XRD spectrum of commercial $CaCO_3$ used as the control showed characteristic diffraction peaks at 11.5°, 20.7°, 23.2°, 29.3°, and 31.4°, as shown in Fig. 10(a). Moreover, the XRD patterns of $CaHPO_4$ derived from *Haliotis* sp. shells matched the XRD patterns of commercial $CaHPO_4$, as shown in Fig. 11 (b). Thus, these results indicate that $CaHPO_4$ was successfully synthesized via a chemical reaction between H_3PO_4 and *Haliotis* sp. shell-derived $CaCO_3$ at pH 6.0.

TCP exists in two major distinct phases α-TCP and β-TCP. α-and β-TCP are currently used as bone graft materials in dentistry, maxillofacial surgery, and orthopedics. β-TCP is mainly applied in the production of biodegradable bioceramics, such as microporous granules and blocks, whereas α-TCP, which is more soluble than β-TCP, is used as bone cement. β-TCP is usually synthesized at lower temperatures than α-TCP [20].

Therefore, to verify the optimal temperature for β-TCP synthesis, the chemical reaction between $CaHPO_4$ and CaO was conducted by sintering at 950, 1000, 1050, and 1100℃ for 3 h. Thereafter, the physiochemical characteristics of the synthesized composites were compared with those of commercial β-TCP using FT-IR and XRD analyses. As shown in Fig. 12(a), the FT-IR spectra of the composites synthesized by sintering at 950 and 1050℃ matched those of commercial β-TCP. On the other hand, the FT-IR spectrum of the composite synthesized by sintering at 1100℃ showed peaks different from those of commercial β-TCP. As shown in Fig. 12(a), β-TCP used as the control is easily identified by a broad band between 900 and 1200 cm^{-1} and by the presence of a peak at 724 cm^{-1}. The peak at 1211 cm^{-1} is characteristic of a non-degenerate deformation of hydrogen groups, such as $H-OPO_3$, $O-PO_3$, and HPO_4^{2-}. However, the absence of a band at 460 cm^{-1}, which is characteristic of α-TCP, is indicative of β-TCP [48]. As shown in Fig. 12(b) - (d), the peak positions of the composites synthesized at 950-1050℃ matched the peak positions of β-TCP used as the control. These results indicated that β-TCP was successfully synthesized by sintering at 950-1050℃ from a mixture of CaO and $CaHPO_4$ derived from *Haliotis* sp. shells. Generally, β-TCP is stable at room temperature and transforms at 1125℃ [60]. Finally, to confirm the synthesis of β-TCP, the XRD pattern of the composite synthesized by sintering at 950℃ was compared with that of commercial β-TCP. As shown in Fig. 13, the physiochemical characteristics of the composite synthesized by sintering at 950℃ matched the characteristics of commercial $CaHPO_4$. Taken together, these data indicate that β-TCP was successfully synthesized by a chemical reaction between $CaHPO_4$ and CaO via sintering at 950 - 1050℃ for 3 h.

HA is attractive for bone regeneration and reconstruction owing to its bone bonding ability and growth promotion property [19]. Therefore, calcium phosphate-based HA biomaterials have been used as the basic biomaterials for replacing and promoting bone growth.

CaO is an important Ca^{2+} resource compound used in the synthesis of bioceramics. In the present study, to synthesize pure CaO, *Haliotis* sp. shells were sintered completely at 950℃ for 3 h. As shown in Fig. 6 and Fig. 7, the FT-IR and XRD results indicate that the physicochemical characteristics of *Haliotis* sp. shell-derived CaO were similar to those of control CaO. This indicates that CaO could be synthesized successfully from *Haliotis* sp. shells. However, a chemical reaction between *Haliotis* sp. shell-derived CaO and phosphoric acid is needed to synthesize HA. In the current study, for the phosphorylation of CaO, the pH of calcium hydroxide was regulated using phosphoric acid at 10.5. Thereafter, the precipitated composite was sintered at 1230℃ for 3 h to synthesize HA. As shown in Fig. 14 and 15, FT-IR spectroscopy and XRD analysis confirmed the material composition and crystallinity of the abalone shell-derived HA.

Alloplasts are synthetic bone graft materials, which can contribute to the repair of defective bones and to the enhancement of bone ingrowth. Today, using synthetic bone graft substitutes composed of bio-ceramic tri-calcium phosphate and hydroxyapatite, it is possible to increase the width, volume, and height of bones in deficient areas to regenerate bone-supporting implant replacements.

In this study, we compared the physicochemical and in vitro biocompatibility characteristics of bone graft substitutes synthesized at a 2 : 8 ratio of HA and β-TCP. The surface morphology and crystal size of the synthesized bone grafting substitutes as defined mixing ratio (2 : 8) of HA and β-TCP were studied under SEM. To observe the electron microscopic structure of bone graft substitutes synthesized from *Haliotis* sp. shell, SEM scanning was performed at an acceleration voltage of 5.5 kV. The Fig. 18. observe the size and shape of each bone graft substitutes at magnified 100X, the surface roughness of the each bone grafting substitutes at the magnified 500X and 1500X and the macroporosity and pore structure of each bone grafting materials at magnified 5000X, respectively. As shown in Fig. 18, micropores with 10 - 100 μm diameter were formatted in both internal and external surface on the all of bone grafting substitutes synthesized by

defined mixing conditions of HA and β-TCP. EDS results showed that the Ca/P ratio value of bone grafting substitutes synthesized from *Haliotis* sp. shell by 2 : 8 mixing ratio of HA and β-TCP is 1.64 that is identical Ca/P ratio of the bone tissue isolated from human body (Fig. 19).

Furthermore, all of synthesized bone grafting substitutes as the defined mixing ratio of HA and β-TCP shown the pH value ranges of 8.6 - 8.8. These pH values of bone grafting substitutes were similar with the physiological optimized pH value of human body. Also, the wettability of each bone grafting substitutes synthesized as defined mixing ratio (2 : 8) of HA and β-TCP. As shown in Table 2, the evaluation of wettability in the performance of dental bone grafts does not have a direct effect. However, in a clinical setting, when a graft is placed, the graft material implanted into the bone can absorb some amount of blood, so that the graft can be located in the bone defect region.

To use as a bone graft material, synthesized *Haliotis* sp. shell-derived bone graft substitutes must have a biological safety. Therefore, the cytotoxicity of eluent prepared from *Haliotis* sp. shell-derived bone graft substitutes was assessed by various methods such as MTT, cell live and dead assay, and DAPI staining. MTT assay showed that the abalone shell-derived *Haliotis* sp. shell-derived bone graft substitutes did not affect the cell viability compared with commercial *Haliotis* sp. shell-derived bone graft substitutes. Furthermore, DAPI staining was performed to verify the cells with nuclear condensation, which is a typical characteristic of apoptosis. However, the apoptotic cells did not observe in the MG-63 cells treated with the eluent prepared from *Haliotis* sp. shell-derived bone graft substitutes. Moreover, to visualize the live (stained as green color) and dead cells (stained as red color), cell live and dead assay was performed. Almost cells treated with the eluent prepared from *Haliotis* sp. shell-derived bone graft substitutes were stained as green color. Taken together, these indicate consistently that *Haliotis* sp. shell-derived bone graft substitutes a high level of biological safety to use as a bone graft material.

Osteoconductivity is one of the most important indicators of functional osteoblasts as differentiated osteoblasts showed much higher mineralization than dental undifferentiated mesenchymal cells [61]. In this study, mineralization of cells cultured with *Haliotis* sp. shell-derived bone graft substitutes and commercial bone graft substitutes effluents was assessed for up to 11 days. As shown in Fig. 24, the mineralized nodules were observed in MG-63 cell cultured with both bone graft substitutes used as control and *Haliotis* sp. shell-derived bone graft substitutes for 7 and 11 days. Although the level of mineralization in MG-63 cells cultured with *Haliotis* sp. shell-derived bone graft substitutes was similar with that of commercial one, these are suggesting that osteoconductivity of *Haliotis* sp. shell-derived bone graft substitutes are at least similar to those used as control one.

To verify whether synthesized *Haliotis* sp. shell-derived bone graft substitutes has a biological and osteoconductive activity in living animals as the *in vivo* test, we generated calvarial bone defection animal model and implanted the synthesized *Haliotis* sp. shell-derived bone graft substitutes into recipient site [62]. After implantation, experimental animals were lived for eight weeks and were sacrificed to analyzed the radiographically evaluation using the X-ray and the Micro-CT. X-ray image analysis indicated that defecting areas on the calvarial bone did not healing yet in experimental animal. While as new bone formation had been observed accordance with synthesized *Haliotis* sp. shell-derived bone graft substitutes implanted into defecting calvarial bone areas of experimental animal. Furthermore, as shown in Fig. 26, Micro-CT image analysis indicated that experimental animal model with the implantation of synthesized *Haliotis* sp. shell-derived bone graft substitutes into the defecting calvarial bone area had been shown the great new bone formation compared with the experimental animals as the control without implantation. Moreover, to confirm the new bone formation in the experimental animals with the implantation of *Haliotis* sp. shell-derived bone graft substitutes, we determined histological the evaluation using both H&E stain and safranin-O & fast green stain. In the H&E staining, *Haliotis* sp. shell-derived

bone graft substitutes implanted into defecting region of calvarial bone did not affect the cell morphology and did not induce the inflammation. Furthermore, in the results of safranin-O & fast green staining, renewal bones located on the under of *Haliotis* sp. shell-derived bone graft substitutes implanted into defecting region of calvarial bone had been stained as green color by fast green reagent.

From the obtained results, it could be confirmed that *Haliotis* sp. shell-derived bone graft substitutes are appropriate for application as bone graft materials in a clinical setting. Therefore, *Haliotis* sp. shell-derived bone graft substitutes with high biocompatibility and optimized physical characteristics are expected to overcome the limitations faced with autologous grafts. Furthermore, owing to their simple manufacturing process, *Haliotis* sp. shell-derived bone graft substitutes can relieve the cost of implant surgery.

Ⅴ. References

1. R.W. Bucholz, A. Carlton, R.E. Holmes, Hydroxyapatite and tricalcium phosphate bone graft substitutes, Orthop Clin North Am 18(2) (1987) 323-34.

2. R.Z. LeGeros, Properties of osteoconductive biomaterials: calcium phosphates, Clin Orthop Relat Res (395) (2002) 81-98.

3. A. John, H.K. Varma, T.V. Kumari, Surface reactivity of calcium phosphate based ceramics in a cell culture system, J Biomater Appl 18(1) (2003) 63-78.

4. G.F. Muschler, S. Negami, A. Hyodo, D. Gaisser, K. Easley, H. Kambic, Evaluation of collagen ceramic composite graft materials in a spinal fusion model, Clin Orthop Relat Res (328) (1996) 250-60.

5. B.L. Eppley, W.S. Pietrzak, M.W. Blanton, Allograft and alloplastic bone substitutes: a review of science and technology for the craniomaxillofacial surgeon, J Craniofac Surg 16(6) (2005) 981-9.

6. J. Clavero, S. Lundgren, Ramus or chin grafts for maxillary sinus inlay and local onlay augmentation: comparison of donor site morbidity and complications, Clin Implant Dent Relat Res 5(3) (2003) 154-60.

7. J.A. McAuliffe, Bone graft substitutes, J Hand Ther 16(2) (2003) 180-7.

8. P.V. Giannoudis, H. Dinopoulos, E. Tsiridis, Bone substitutes: an update, Injury 36 Suppl 3 (2005) S20-7.

9. C. Mueller, B. Muller, A.P. Perruchoud, Biomarkers: past, present, and future, Swiss Med Wkly 138(15-16) (2008) 225-9.

10. K.H. Knese, [Bone Formation and Development of Osseous Structure], Verh Dtsch Ges Pathol 47 (1963) 35-54.

11. U. Breine, P.I. Branemark, Reconstruction of alveolar jaw bone. An experimental

and clinical study of immediate and preformed autologous bone grafts in combination with osseointegrated implants, Scand J Plast Reconstr Surg 14(1) (1980) 23-48.

12. C. Dahlin, A. Linde, J. Gottlow, S. Nyman, Healing of bone defects by guided tissue regeneration, Plast Reconstr Surg 81(5) (1988) 672-6.

13. R.K. Schenk, D. Buser, W.R. Hardwick, C. Dahlin, Healing pattern of bone regeneration in membrane-protected defects: a histologic study in the canine mandible, Int J Oral Maxillofac Implants 9(1) (1994) 13-29.

14. Y. Wan, H. Wu, A. Yu, D. Wen, Biodegradable polylactide/chitosan blend membranes, Biomacromolecules 7(4) (2006) 1362-72.

15. T. Albrektsson, C. Johansson, Osteoinduction, osteoconduction and osseointegration, Eur Spine J 10 Suppl 2 (2001) S96-101.

16. C. Tudor, S. Srour, M. Thorwarth, P. Stockmann, F.W. Neukam, E. Nkenke, K.A. Schlegel, E. Felszeghy, Bone regeneration in osseous defects-application of particulated human and bovine materials, Oral Surg Oral Med Oral Pathol Oral Radiol Endod 105(4) (2008) 430-6.

17. W.R. Moore, S.E. Graves, G.I. Bain, Synthetic bone graft substitutes, ANZ J Surg 71(6) (2001) 354-61.

18. P.D. Costantino, C.D. Friedman, Synthetic bone graft substitutes, Otolaryngol Clin North Am 27(5) (1994) 1037-74.

19. T.J. Cypher, J.P. Grossman, Biological principles of bone graft healing, J Foot Ankle Surg 35(5) (1996) 413-7.

20. H.F. Nasr, M.E. Aichelmann-Reidy, R.A. Yukna, Bone and bone substitutes, Periodontol 2000 19 (1999) 74-86.

21. M.G. Donovan, N.C. Dickerson, J.C. Mitchell, Calvarial bone harvest and

grafting techniques for maxillary and mandibular implant surgery, Atlas Oral Maxillofac Surg Clin North Am 2(2) (1994) 109-22.

22. A.P. White, Lumbar spinal fusion rates as influenced by bone grafts and bone graft alternatives: a critical appraisal of common clinical and radiographic comparative methodologies, Spine J 9(11) (2009) 916-8.

23. P. Tayapongsak, J.A. Wimsatt, J.P. LaBanc, M.F. Dolwick, Morbidity from anterior ilium bone harvest. A comparative study of lateral versus medial surgical approach, Oral Surg Oral Med Oral Pathol 78(3) (1994) 296-300.

24. B.D. Ratner, S.J. Bryant, Biomaterials: where we have been and where we are going, Annu Rev Biomed Eng 6 (2004) 41-75.

25. G. Carter, Harvesting and implanting allograft bone, AORN J 70(4) (1999) 660-70; quiz 672-6.

26. S. Stevenson, Biology of bone grafts, Orthop Clin North Am 30(4) (1999) 543-52.

27. G.E. Friedlaender, D.M. Strong, W.W. Tomford, H.J. Mankin, Long-term follow-up of patients with osteochondral allografts. A correlation between immunologic responses and clinical outcome, Orthop Clin North Am 30(4) (1999) 583-8.

28. D.M. Ehrler, A.R. Vaccaro, The use of allograft bone in lumbar spine surgery, Clin Orthop Relat Res (371) (2000) 38-45.

29. J. Skowronski, Tactics in the treatment of fractures of the distal epiphysis of the radial bone, Ortop Traumatol Rehabil 5(1) (2003) 70-9.

30. C.J. Damien, J.R. Parsons, Bone graft and bone graft substitutes: a review of current technology and applications, J Appl Biomater 2(3) (1991) 187-208.

31. J.O. Hollinger, J. Brekke, E. Gruskin, D. Lee, Role of bone substitutes, Clin

Orthop Relat Res (324) (1996) 55-65.

32. J.F. Keating, M.M. McQueen, Substitutes for autologous bone graft in orthopaedic trauma, J Bone Joint Surg Br 83(1) (2001) 3-8.

33. S.H. Palmer, C.L. Gibbons, N.A. Athanasou, The pathology of bone allograft, J Bone Joint Surg Br 81(2) (1999) 333-5.

34. T.A. Einhorn, Enhancement of fracture-healing, J Bone Joint Surg Am 77(6) (1995) 940-56.

35. F.G. Emmings, Chemically modified osseous material for the restoration of bone defects, J Periodontol 45(5) (1974) 385-90.

36. B. Wenz, B. Oesch, M. Horst, Analysis of the risk of transmitting bovine spongiform encephalopathy through bone grafts derived from bovine bone, Biomaterials 22(12) (2001) 1599-606.

37. K.U. Lewandrowski, J.D. Gresser, D.L. Wise, D.J. Trantol, Bioresorbable bone graft substitutes of different osteoconductivities: a histologic evaluation of osteointegration of poly(propylene glycol-co-fumaric acid)-based cement implants in rats, Biomaterials 21(8) (2000) 757-64.

38. J.G. Zhao, Q.Q. Yan, R.Y. Xue, J. Zhang, Y.Q. Zhang, Isolation and identification of colourless caffeoyl compounds in purple sweet potato by HPLC-DAD-ESI/MS and their antioxidant activities, Food Chem 161 (2014) 22-6.

39. G. Fu, S. Valiyaveettil, B. Wopenka, D.E. Morse, CaCO3 biomineralization: acidic 8-kDa proteins isolated from aragonitic abalone shell nacre can specifically modify calcite crystal morphology, Biomacromolecules 6(3) (2005) 1289-98.

40. M. Lichovnikova, The effect of dietary calcium source, concentration and particle size on calcium retention, eggshell quality and overall calcium

requirement in laying hens, Br Poult Sci 48(1) (2007) 71-5.

41. A.C. Tas, Monetite (CaHPO4) Synthesis in Ethanol at Room Temperature, J Am Ceram Soc 92(12) (2009) 2907-2912.

42. B. Aksakal, M. Kom, H.B. Tosun, M. Demirel, Influence of micro- and nano-hydroxyapatite coatings on the osteointegration of metallic (Ti6Al4 V) and bioabsorbable interference screws: an in vivo study, Eur J Orthop Surg Traumatol 24(5) (2014) 813-9.

43. X. Zeng, W. Wei, X. Li, J. Zeng, L. Wu, Direct electrochemistry and electrocatalysis of hemoglobin entrapped in semi-interpenetrating polymer network hydrogel based on polyacrylamide and chitosan, Bioelectrochemistry 71(2) (2007) 135-41.

44. J.Z. Liang, Mechanical Properties of PPS/PC/GF/Nano-CaCO3 Hybrid Composites, Polym-Plast Technol 48(3) (2009) 292-296.

45. L. Zhang, L.H. Yue, F. Wang, Q. Wang, Divisive effect of alcohol-water mixed solvents on growth morphology of calcium carbonate crystals, J Phys Chem B 112(34) (2008) 10668-74.

46. G. Cama, B. Gharibi, M.S. Sait, J.C. Knowles, A. Lagazzo, S. Romeed, L. Di Silvio, S. Deb, A novel method of forming micro- and macroporous monetite cements, J Mater Chem B 1(7) (2013) 958-969.

47. V.P. Feitosa, M.G. Bazzocchi, A. Putignano, G. Orsini, A.L. Luzi, M.A.C. Sinhoreti, T.F. Watson, S. Sauro, Dicalcium phosphate (CaHPO4 center dot 2H(2)O) precipitation through ortho- or meta-phosphoric acid-etching: Effects on the durability and nanoleakage/ultra-morphology of resin-dentine interfaces, J Dent 41(11) (2013) 1068-1080.

48. D. Zhu, J. Zhang, Y. Bin, C. Xu, J. Shen, M. Matsuo, Dielectric studies on the heterogeneity and interfacial property of composites made of polyacene quinone

radical polymers and sulfonated polyurethanes, J Phys Chem A 116(9) (2012) 2024-31.

49. S. Sakai, T. Anada, K. Tsuchiya, H. Yamazaki, H.C. Margolis, O. Suzuki, Comparative study on the resorbability and dissolution behavior of octacalcium phosphate, beta-tricalcium phosphate, and hydroxyapatite under physiological conditions, Dent Mater J 35(2) (2016) 216-224.

50. P.M.S.L. Shanthi, R.V. Mangalaraja, A.P. Uthirakumar, S. Velmathi, T. Balasubramanian, M. Ashok, Synthesis and characterization of porous shell-like nano hydroxyapatite using Cetrimide as template, J Colloid Interf Sci 350(1) (2010) 39-43.

51. C.H.F. Hammerle, R.E. Jung, D. Yaman, N.P. Lang, Ridge augmentation by applying bioresorbable membranes and deproteinized bovine bone mineral: a report of twelve consecutive cases, Clin Oral Implan Res 19(1) (2008) 19-25.

52. T. Nakazawa, M. Takaso, T. Imura, K. Adachi, K. Fukushima, W. Saito, G. Miyajima, A. Minatani, R. Shinntani, M. Itoman, K. Takahashi, M. Yamazaki, S. Ohtori, A. Sasaki, Autogenous iliac crest bone graft versus banked allograft bone in scoliosis surgery in patients with Duchenne muscular dystrophy, Int Orthop 34(6) (2010) 855-861.

53. K. Bechara, A.M. Dottore, P.Y. Kawakami, S.A. Gehrke, P.G. Coelho, A. Piattelli, G. Iezzi, J.A. Shibli, A histological study of non-ceramic hydroxyapatite as a bone graft substitute material in the vertical bone augmentation of the posterior mandible using an interpositional inlay technique: A split mouth evaluation, Ann Anat 202 (2015) 1-7.

54. V. Stanic, N.N. Aldini, M. Fini, G. Giavaresi, R. Giardino, A. Krajewski, A. Ravaglioli, M. Mazzocchi, B. Dubini, M.G. Bossi, F. Rustichelli, Osteointegration of bioactive glass-coated zirconia in healthy bone: an in vivo evaluation, Biomaterials 23(18) (2002) 3833-41.

55. D.E. Tallman, K.L. Levine, C. Siripirom, V.G. Gelling, G.P. Bierwagen, S.G. Croll, Nanocomposite of polypyrrole and alumina nanoparticles as a coating filler for the corrosion protection of aluminium alloy 2024-T3, Appl Surf Sci 254(17) (2008) 5452-5459.

56. S. Marchant, P.A. Haye, S.A. Marin, F.M. Winkler, Genetic variability revealed with microsatellite markers in an introduced population of the abalone Haliotis discus hannai Ino, Aquac Res 40(3) (2009) 298-304.

57. H. Chen, K. Mai, W. Zhang, Z. Liufu, W. Xu, B. Tan, Effects of dietary pyridoxine on immune responses in abalone, Haliotis discus hannai Ino, Fish Shellfish Immunol 19(3) (2005) 241-52.

58. D. Shan, S.X. Wang, H.G. Xue, S. Cosnier, Direct electrochemistry and electrocatalysis of hemoglobin entrapped in composite matrix based on chitosan and CaCO3 nanoparticles, Electrochem Commun 9(4) (2007) 529-534.

59. C. Moseke, U. Gbureck, Tetracalcium phosphate: Synthesis, properties and biomedical applications, Acta Biomater 6(10) (2010) 3815-3823.

60. R.G. Carrodeguas, S. De Aza, alpha-Tricalcium phosphate: Synthesis, properties and biomedical applications, Acta Biomater 7(10) (2011) 3536-3546.

61. Y. Chen, H.C. Whetstone, A.C. Lin, P. Nadesan, Q. Wei, R. Poon, B.A. Alman, Beta-catenin signaling plays a disparate role in different phases of fracture repair: implications for therapy to improve bone healing, PLoS Med 4(7) (2007) e249.

62. W.S. Song, C.S. Kim, S.H. Choi, G.J. Jhon, H.Y. Kim, K.S. Cho, C.K. Kim, J.K. Chai, The effects of a bioabsorbable barrier membrane containing safflower seed extracts on periodontal healing of 1-wall intrabony defects in beagle dogs, J Periodontol 76(1) (2005) 22-33.

감사의 글

이 논문이 완성 될 수 있도록 도와주신 주위의 모든 분들께 감사의 말씀 전합니다. 석·박사 학위 동안 이끌어주시고 따뜻한 사랑을 베풀어주신 존경하는 김수관 교수님께 진심으로 감사드립니다. 또한 바쁘신 와중에도 부족한 논문의 문제점과 미비점을 바로 잡아주신 서울대학교 김영균 교수님께 감사를 드립니다. 언제나 가까이에서 애정으로 지도해주시고, 끊임없는 격려와 조언을 해주신 이숙영 교수님께도 깊은 감사의 말씀을 전합니다. 그리고 힘들어 할 때나, 고민이 있을 때, 늘 곁에서 아낌없고 현질적인 격려를 통해 도움을 주시고, 한 순간의 좌절이 견디기 힘들고 나태해질 때, 다양한 기회와 조언으로 일깨워 주신 김재성 교수님께 항상 감사드립니다. 그리고 학위 과정 간 애정으로 지도해 주시고, 부족한 저에게 언제나 학문적, 인성적으로 많은 가르침을 주셨던 김도경 교수님 정말 감사드립니다.

저를 친동생처럼 아껴주고, 과분한 애정과 다양한 경험으로 저를 성장 시켜준 중국의 우리 형 박정강, 광주의 우리 형 진승찬 두 분의 형님들 감사드립니다. 처음부터 함께하며, 언제나 의지해 왔던 선배이자 후배인 조인아 선생님과 함께 마무리를 할 수 있어서 정말 기쁘게 생각합니다. 긍정적으로 연구실의 모범이 되어주고 있는 정서윤, 김태현, 임향이 선생님, 그리고 수년간 함께 했던 연구실의 모든 선후배 동료 선생님들께 감사드립니다.

이 순간까지 많은 격려와 조언으로 저를 일깨워 주신 김춘성 교수님, 문성민 박사님의 가르침과 지도 덕분에 많은 것을 배울 수 있었습니다. 언제나 감사하고, 앞으로도 두려움 없이 도전 할 수 있는 사람으로 한걸음씩 천천히 나아가도록 하겠습니다.

끝으로 오늘에 이르기까지 부족한 자식을 한없는 사랑과 희생으로 가르치시고 보살펴 주신, 세상에서 가장 존경하며 사랑하는 우리 아버지 강성철님, 김명옥 여사님. 항상 아들을 이끌어주시고 믿음으로 지켜봐 주셔서 감사합니다. 더욱 열심히 새롭게 정진 할 것을 다짐하며 사랑하는 부모님께 이 글을 바칩니다.

2018년 마지막 논문 편집을 마치며

강 경 록